Materials and methods

This investigation conforms with the *Guide for the Care and Use of Laboratory Animals* published by the US National Institutes of Health (NIH Publication No. 85-23, revised 1996).

Surgical preparation

Twenty-four adult cats weighing from 2.2 to 3.8 kg were anesthetized by an intraperitoneal injection of pentobarbital sodium (30–35 mg/kg) and ventilated mechanically with room air mixed with oxygen. The depth of anesthesia was maintained with a continuous intravenous infusion of pentobarbital sodium (1–2 mg kg^{-1} h^{-1}) through a catheter inserted from the right femoral vein to the inferior vena cava. Systemic arterial pressure (AP) was monitored from a catheter inserted from the right femoral artery into the abdominal aorta. Heart rate (HR) was determined from an electrocardiogram using a cardiotachometer. Esophageal temperature of the animal was measured using a thermometer (CTM-303, TERUMO, Japan) and was maintained at around 37 °C using a heated pad and a lamp.

Bilateral vagal nerves were sectioned through a midline cervical incision. With the animal in the lateral position, the left fifth and sixth ribs were resected to expose the heart. A dialysis probe was implanted, using a fine guiding needle, into the anterolateral free wall of the left ventricle perfused by the left anterior descending coronary artery (LAD). A 3-0 silk suture was passed around the LAD just distal to the first diagonal branch for later coronary occlusion. When an experimental protocol required electrical stimulation of the vagal efferent nerves, bipolar platinum electrodes were attached to the cardiac end of sectioned vagal nerves bilaterally. The nerves and electrodes were covered with warmed mineral oil for insulation. When an experimental protocol required cardiac pacing, bipolar stainless-steel wire electrodes were sutured at the left ventricular apex away from the implanted dialysis probe. Heparin sodium (100 U/kg) was administered intravenously to prevent blood coagulation.

In additional four anesthetized cats, the left ventricle was implanted with a dialysis probe and a pair of pacing electrodes to examine the effects of left ventricular pacing alone on the myocardial interstitial NE levels. The dialysis probe and pacing leads were placed in the same manner as described in the previous paragraph.

At the end of the experiment, the experimental animals were killed with an overdose of pentobarbital sodium. Postmortem examination confirmed that the dialysis probe had been implanted within the left ventricular myocardium.

Dialysis technique

The materials and properties of the dialysis probe have been previously described (Akiyama et al., 1991, 1994). Briefly, we designed a transverse dialysis probe. A dialysis fiber (13 mm length, 310 μm O.D., 200 μm I.D.; PAN-1200, 50,000 molecular weight cutoff, Asahi Chemical, Japan) was glued at both ends to polyethylene tubes (25 cm length, 500 μm O.D., 200 μm I.D.). The dialysis probe was perfused at a rate of 2 μl/min with Ringer solution containing the cholinesterase inhibitor eserine (100 μM). Dialysate sampling was initiated 2 h after implanting the dialysis probe, when the dialysate concentrations of NE and ACh had reached steady states (Akiyama et al., 1991, 1994). The actual dialysate sampling lagged behind a given collection period by 5 min taking into account the dead space volume between the dialysis membrane and the sample tube. Dialysate concentrations of NE and ACh were measured separately by high performance liquid chromatography with electrochemical detection (DTA-300, Eicom, Japan). Details of the NE and ACh measurements have been previously described (Akiyama et al., 1991, 1994).

Protocols

Protocol 1 (VX, n = 8)

As a control experiment, we measured ischemia-induced NE and ACh releases during 60-min LAD occlusion in vagotomized animals. After collecting a 15-min baseline dialysate sample, we occluded the LAD for 60 min and collected four consecutive 15-min dialysate samples during acute myocardial ischemia. We then loosened the LAD snare and collected a 15-min dialysate sample during reperfusion.

Protocol 2 (VS, n = 8)

We examined the effects of vagal stimulation on ischemia-induced NE and ACh releases. To avoid possible preconditioning mimetic effects of ACh released by vagal stimulation (Przyklenk and Kloner, 1995; Kawada et al., 2002a), we initiated the bilateral vagal stimulation (5 Hz, 1 ms in pulse duration and 10 V in pulse amplitude) at the onset of LAD occlusion. The vagal stimulation continued for the 60-min ischemic period and the 15-min reperfusion period.

Protocol 3 (VSP, n = 8)

To eliminate the effects of bradycardia associated with vagal stimulation, we performed vagal stimulation under fixed-rate pacing conditions. We initiated the bilateral vagal stimulation (5 Hz, 1 ms in pulse duration and 10 V in pulse amplitude) and paced the heart from the onset of LAD occlusion to the conclusion of the experimental period. The ventricular pacing rate was set close to the HR recorded immediately before the LAD occlusion.

Supplemental protocol (n = 4)

To examine the effects of left ventricular pacing on the myocardial interstitial NE levels, we collected 15-min dialysate samples under control conditions as well as under left ventricular pacing at 170 beats/min.

Statistical analysis

All data are presented as means ± SE values. In each group, the effects of LAD occlusion on dialysate concentrations of NE and ACh were examined using a repeated-measures analysis of

variance followed by a Dunnett test against respective baseline concentrations. Because the variance of NE data was very large and increased with mean, the NE data were compared after the logarithmic transform (Snedecor and Cochran, 1989). Differences were considered significant at $P<0.05$. To examine the effects of vagal stimulation with or without the ventricular pacing, dialysate concentrations of NE and ACh were compared among the three groups at each corresponding time period using one-way analysis of variance followed by a Student–Newman–Keuls test for all pairwise comparisons (Glantz, 2002). The NE data were compared after the logarithmic transform. Differences were considered significant at $P<0.05$. Heart rate and mean AP were determined immediately before the coronary occlusion (designated as time 0), after 5, 10, 15, 30, 45, and 60 min of the occlusion, and after 15 min of reperfusion. One-way analysis of variance followed by a Student–Newman–Keuls test was also applied to compare HR and mean AP among the three groups at each time point.

Results

Fig. 1 depicts LAD occlusion-induced myocardial interstitial NE accumulation within the ischemic zone. The inset shows the NE levels during baseline conditions in a magnified ordinate. In the VX group, LAD occlusion increased the NE level approximately 200 fold compared to the baseline level at 45–60 min. This occlusion-induced NE accumulation was significantly suppressed in the VS group compared with the VX group in 15–30, 30–45, and 45–60 min time periods. The difference between the VS and VX groups did not reach statistical significance at the reperfusion period. In the VSP group, in which HR was kept constant, vagal stimulation did not attenuate the occlusion-induced NE accumulation. In the supplemental protocol, the baseline myocardial interstitial NE level was 0.17±0.01 nM. The NE level during ventricular pacing at 170 beats/min was 0.21±0.09 nM.

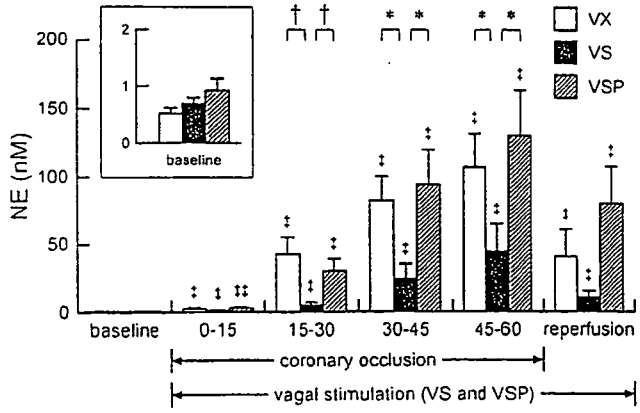

Fig. 1. Coronary occlusion-induced norepinephrine (NE) accumulation in the ischemic myocardium. VX: vagotomy, VS: vagal stimulation, VSP: vagal stimulation with ventricular pacing. The inset shows the baseline conditions with a magnified ordinate. Data are means±SE. ‡$P<0.01$ and ‡‡$P<0.05$ from the corresponding baseline value in each group. †$P<0.01$ and *$P<0.05$ by all pairwise comparisons among the three groups.

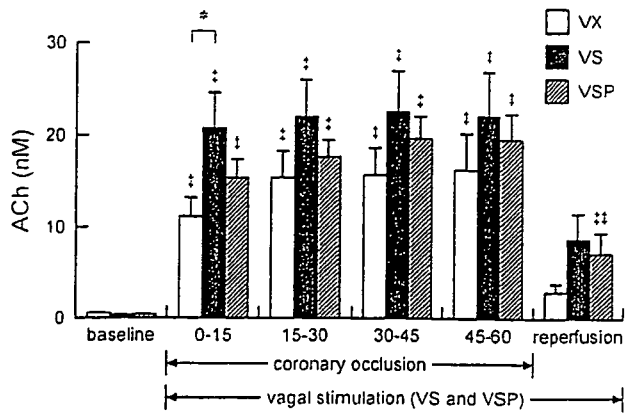

Fig. 2. Coronary occlusion-induced acetylcholine (ACh) accumulation in the ischemic myocardium. Data are means±SE. ‡$P<0.01$ and ‡‡$P<0.05$ from the corresponding baseline value in each group. *$P<0.05$ by all pairwise comparisons among the three groups.

Fig. 2 shows LAD occlusion-induced myocardial interstitial ACh accumulation within the ischemic zone. In the VX group, LAD occlusion increased the ACh level approximately 20 times higher than the baseline level at 45–60 min. The ACh level at 0–15 min was significantly higher in the VS than the VX group. For the rest of the ischemic period and reperfusion period, the differences between the VS and VX groups were not significant. The ACh levels in the VSP group did not differ from the VX group for any of the sampling periods.

Fig. 3 summarizes changes in HR and mean AP. In the VS group, HR was decreased by approximately 80 beats/min compared with the VX group at 5 min of coronary occlusion. The HR decrease continued for the rest of the ischemic period and reperfusion period. In the VSP group, HR was kept close to the preocclusion level, and it did not differ from the VX group

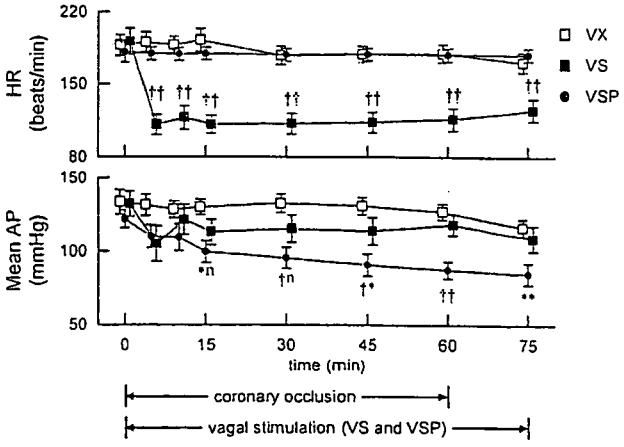

Fig. 3. Time courses of heart rate (HR) and mean arterial pressure (AP) during 60-min ischemia and 15-min reperfusion. The baseline values obtained just before coronary occlusion are plotted at time 0. Data points for VX and VSP groups are slightly displaced along the time axis for better view of overlapping points. Data are means±SE. In the HR data, †† represents statistical significance of $P<0.01$ from both the VX and VSP groups by all pairwise comparisons. In the AP data, when two characters are added to the VSP data point, the first and second characters represent the statistical significance from VX and VS groups, respectively. *, †, and n designate $P<0.05$, $P<0.01$, and "not significant", respectively.

for all the time points. Mean AP did not differ statistically between VX and VS groups. Mean AP in the VSP group progressively decreased and became significantly lower than the VX group after 15 min of the ischemic period. Mean AP in the VSP group was also significantly lower than the VS group after 45 min of the ischemic period.

Discussion

We have shown that electrical vagal stimulation suppressed ischemia-induced NE release and enhanced an initial increase in the ACh levels in the ischemic myocardium. Fixed-rate pacing abolished the suppression of ischemia-induced NE release by vagal stimulation in the present experimental settings.

Effects of vagal stimulation on ischemia-induced NE release

Several mechanisms can be put forward to explain the suppression of ischemia-induced myocardial interstitial NE release by vagal stimulation. First, activation of presynaptic muscarinic receptors on the sympathetic nerve endings inhibits the exocytotic NE release under normal physiological conditions (Levy and Blattberg, 1976). However, the presynaptic inhibition is unlikely the mechanism underlying the vagally mediated suppression of the ischemia-induced NE release because of the following reasons. Although the exocytotic release mechanism participates in the ischemia-induced NE release within the first 20 min of ischemia, the non-exocytotic release mechanism becomes predominant as the ischemic period is prolonged (Akiyama and Yamazaki, 1999). Myocardial ischemia gradually depletes ATP in the ischemic region including sympathetic nerve terminals, which leads to accumulation of axoplasmic NE and reduction of normal Na^+gradient across the plasma membrane in the sympathetic nerve terminals. The NE uptake transporter on the sympathetic nerve terminals, driven by the Na^+gradient, is then reversed, evoking non-exocytotic NE release (Schwartz, 2000). Therefore, the presynaptic inhibition of exocytotic NE release might contribute little to the suppression of ischemia-induced NE release during prolonged ischemia. Furthermore, the presynaptic inhibition of exocytotic NE release becomes less effective during the ischemic insult (Du et al., 1990; Haunstetter et al., 1994). The fact that the ischemia-induced NE release did not differ between the VSP and VX groups is also in opposition to the presynaptic inhibition as a chief mechanism underlying the vagally mediated suppression of ischemia-induced NE release (Fig. 1). Although left ventricular pacing could have affected myocardial interstitial NE levels, the results of the supplemental protocol indicates that changes in the NE levels by ventricular pacing might be negligibly small compared to the ischemia-induced NE release.

Second, the suppression of ischemia-induced NE release by vagal stimulation may be related to myocardial protection via direct vasodiation of the coronary artery. The coronary dilation may enhance collateral flow in the ischemic region and protect against myocardial deterioration evoked by ischemia. Both ACh and vasoactive intestinal polypeptide (VIP) are known to exert direct coronary dilation (Feliciano and Henning, 1998; Gross et al., 1981; Henning and Sawmiller, 2001). VIP is colocalized with ACh in the postganglionic vagal fibers and is released by high-frequency (20 Hz) vagal stimulation. VIP may interact with NE transport or exocytosis like nociceptin (Yamazaki et al., 2001). However, fixed-rate pacing abolished the ability of vagal stimulation to suppress the ischemia-induced NE release. Hence the direct coronary vasodilation and/or interaction with the sympathetic system via VIP might have played little role in suppressing ischemia-induced NE release in the present experimental settings. Another factor that should be taken into account is that the relatively low-frequency (5 Hz) stimulation might have limited the amount of VIP release from the vagal nerve endings.

Third, HR is one of the most important determinants of myocardial oxygen consumption (Mohrman and Heller, 1997). In the present study, HR in the VS group decreased to approximately 60% that of the VX group during the ischemic period (Fig. 3), which slowed the energy consumption of the myocardium. Bradycardia might also decrease ventricular contractility via a force-frequency mechanism (Maughan et al., 1985). In addition, bradycardia may increase coronary perfusion via prolongation of diastolic interval (Buck et al., 1981). These factors slowed energy consumption in the ischemic region including sympathetic nerve terminals, delaying the time course for non-exocytotic NE release. The prevention of excess NE would further reduce myocardial oxygen consumption and decelerate the progression of ischemic injury (Suga et al., 1983). The ischemia-induced NE release did not differ between the VSP and VX groups despite the lower mean AP in the VSP compared with the VX group. Although lowering AP might decrease afterload of the ventricle and reduce energy consumption, the beneficial effect of afterload reduction might have been masked in the VSP group due to inefficient cardiac pumping function associated with asynchrony between sinus rate and ventricular rate. Proper atrioventricular conduction time contributes to the ventricular filling (Meisner et al., 1985). In the VSP group, the sinus rate was reduced by vagal stimulation whereas the ventricular rate was maintained by fixed-rate pacing. Dissociation of the sinus rate and ventricular rate might have impaired the ventricular filling to a variable extent, resulting in a progressive reduction in AP.

Finally, the vagal stimulation decreases ventricular contractile force against sympathetic activation via the direct projections to the ventricle (Nakayama et al., 2001). This mechanism might have also contributed to the reduction of the myocardial oxygen consumption and slowed the progression of ischemic injury in the VS group. However, the ventricular pacing canceled the protective effects in the VSP group, possibly by the adverse influences discussed in the previous paragraph. Further studies are required to isolate the factor(s) most important for the suppression of ischemia-induced NE release by the vagal stimulation.

Effects of vagal stimulation on ischemia-induced ACh release

In contrast to the suppressive effect of NE release, vagal nerve stimulation can exert two opposing influences on ACh release in the ischemic myocardium. The nerve stimulation itself induces exocytotic ACh release from nerve endings. Acute myocardial ischemia impairs conduction of the nerves traversing in the ischemic region (Barber et al., 1983; Inoue and Zipes, 1988; Martins et al., 1989). Acute myocardial ischemia also impairs the exocytotic ACh release in the postischemic myocardium (Kawada et al., 2002b). On the other hand, acute myocardial ischemia causes myocardial ACh release in the ischemic region via a local release mechanism independent of efferent nerve activity (Kawada et al., 2000). Hence, the amount of ACh release was net effects of ACh release evoked by nerve stimulation and ischemia; vagally mediated protection against ischemic injury should augment the former and attenuate the latter.

Although vagal stimulation augmented myocardial interstitial ACh release during the 0–15 min period of coronary occlusion in the VS group than in the VX group, the initial enhancement was not observed in the VSP group. One possible mechanism for the difference in the initial ACh release between the VS and VSP groups is that the progression of ischemia in the VSP group relative to the VS group impaired the vagal nerve conduction in the ischemic region, reducing the exocytotic ACh release. The other possible mechanism is that the high levels of NE might have attenuated the stimulation-induced ACh release from the vagal nerve endings via α-adrenergic mechanisms (Akiyama and Yamazaki, 2000).

There are several limitations to the present study. First, we avoided large myocardial ischemia by occluding LAD just distal to the first diagonal branch. Accordingly, the incidence of lethal ventricular arrhythmia was too low to draw any conclusion as to the effects of vagal stimulation on the arrhythmogenesis. Further studies with larger myocardial ischemia are clearly required to examine the effects of vagal stimulation on the incidence of lethal ventricular arrhythmia in relation to the observed NE and/or ACh levels in the ischemic myocardium. Second, plasma catecolamine levels might have been increased during the LAD occlusion, which might affect HR and cardiac function in the non-ischemic region. Although changes in plasma catecholamine levels may play significant roles in determining systemic hemodynamics, the ischemic region was only poorly perfused. Accordingly, direct effects of plasma catecholamines on the myocardial interstitial NE and ACh levels in the ischemic region might have been limited in the present study.

Conclusion

Electrical vagal stimulation suppressed ischemia-induced NE release in the ischemic myocardium in anesthetized cats. The vagal stimulation augmented ischemia-induced ACh release at the 0–15 min period of ischemia. Although acute myocardial ischemia causes myocardial NE and ACh releases independent of efferent nerve activity, the vagal stimulation was able to modulate both NE and ACh levels in the ischemic region. The suppression of NE release and augmentation of initial ACh release in the ischemic myocardium by vagal stimulation may reduce the ischemic injury to the heart. The direct neural intervention could be a new modality of medical engineering to cope with ischemic heart diseases.

Acknowledgments

This study was supported by Health and Labour Sciences Research Grant for Research on Advanced Medical Technology (H14-Nano-002) from the Ministry of Health Labour and Welfare of Japan, by Grant-in-Aid for Scientific Research (C-15590786) from the Ministry of Education, Science, Sports and Culture of Japan, and by the Program for Promotion of Fundamental Studies in Health Science from the Organization for Pharmaceutical Safety and Research.

References

Akiyama, T., Yamazaki, T., 1999. Norepinephrine release from cardiac sympathetic nerve endings in the in vivo ischemic region. Journal of Cardiovascular Pharmacology 34, S11–S14.

Akiyama, T., Yamazaki, T., 2000. Adrenergic inhibition of endogenous acetylcholine release on postganglionic cardiac vagal nerve terminals. Cardiovascular Research 46, 531–538.

Akiyama, T., Yamazaki, T., Ninomiya, I., 1991. In vivo monitoring of myocardial interstitial norepinephrine by dialysis technique. American Journal of Physiology. Heart and Circulatory Physiology 261, H1643–H1647.

Akiyama, T., Yamazaki, T., Ninomiya, I., 1994. In vivo detection of endogenous acetylcholine release in cat ventricles. American Journal of Physiology. Heart and Circulatory Physiology 266, H854–H860.

Armour, J.A., 1999. Myocardial ischaemia and the cardiac nervous system. Cardiovascular Research 41, 41–54.

Barber, M.J., Mueller, T.M., Henry, D.P., Felten, S.Y., Zipes, D.P., 1983. Transmural myocardial infarction in the dog produces sympathectomy in noninfarcted myocardium. Circulation 67, 787–796.

Buck, J.D., Warltier, D.C., Hardman, H.F., Gross, G.J., 1981. Effects of sotalol and vagal stimulation on ischemic myocardial blood flow distribution in the canine heart. Journal of Pharmacological and Experimental Therapeutics 216, 347–351.

Du, X.J., Dart, A.M., Riemersma, R.A., Oliver, M.F., 1990. Failure of the cholinergic modulation of norepinephrine release during acute myocardial ischemia in the rat. Circulation Research 66, 950–956.

Feliciano, L., Henning, R.J., 1998. Vagal nerve stimulation releases vasoactive intestinal peptide which significantly increases coronary artery blood flow. Cardiovascular Research 40, 45–55.

Glantz, S.A., 2002. Primer of Biostatistics, 5th ed. McGraw-Hill, New York.

Gross, G.J., Buck, J.D., Warltier, D.C., 1981. Transmural distribution of blood flow during activation of coronary muscarinic receptors. American Journal of Physiology. Heart and Circulatory Physiology 240, H941–H946.

Haunstetter, A., Haass, M., Yi, X., Krüger, C., Kübler, W., 1994. Muscarinic inhibition of cardiac norepinephrine and neuropeptide Y release during ischemia and reperfusion. American Journal of Physiology. Regulatory, Integrative and Comparative Physiology 267, R1552–R1558.

Henning, R.J., Sawmiller, D.R., 2001. Vasoactive intestinal peptide: cardiovascular effects. Cardiovascular Research 49, 27–37.

Inoue, H., Zipes, D.P., 1988. Time course of denervation of efferent sympathetic and vagal nerves after occlusion of the coronary artery in the canine heart. Circulation Research 62, 1111–1120.

Kawada, T., Yamazaki, T., Akiyama, T., Sato, T., Shishido, T., Inagaki, M., Takaki, H., Sugimachi, M., Sunagawa, K., 2000. Differential acetylcholine release mechanisms in the ischemic and non-ischemic myocardium. Journal of Molecular and Cellular Cardiology 32, 405–414.

Kawada, T., Yamazaki, T., Akiyama, T., Inagaki, M., Shishido, T., Zheng, C., Yanagiya, Y., Sugimachi, M., Sunagawa, K., 2001. Vagosympathetic interactions in ischemia-induced myocardial norepinephrine and acetylcholine release. American Journal of Physiology. Heart and Circulatory Physiology 280, H216–H221.

Kawada, T., Yamazaki, T., Akiyama, T., Mori, H., Inagaki, M., Shishido, T., Takaki, H., Sugimachi, M., Sunagawa, K., 2002. Effects of brief ischaemia on myocardial acetylcholine and noradrenaline levels in anaesthetized cats. Autonomic Neuroscience 95, 37–42.

Kawada, T., Yamazaki, T., Akiyama, T., Mori, H., Uemura, K., Miyamoto, T., Sugimachi, M., Sunagawa, K., 2002. Disruption of vagal efferent axon and nerve terminal function in the postischemic myocardium. American Journal of Physiology. Heart and Circulatory Physiology 283, H2687–H2691.

Lameris, T.W., de Zeeuw, Sandra, Alberts, G., Boomsma, F., Duncker, D.J., Verdouw, P.D., Veld, A.J., van den Meiracker, A.H., 2000. Time course and mechanism of myocardial catecholamine release during transient ischemia in vivo. Circulation 101, 2645–2650.

Levy, M.N., Blattberg, B., 1976. Effect of vagal stimulation on the overflow of norepinephrine into the coronary sinus during cardiac sympathetic nerve stimulation in the dog. Circulation Research 38, 81–84.

Li, M., Zheng, C., Sato, T., Kawada, T., Sugimachi, M., Sunagawa, K., 2004. Vagal nerve stimulation markedly improves long-term survival after chronic heart failure in rats. Circulation 109, 120–124.

Martins, J.B., Lewis, R., Wendt, D., Lund, D.D., Schmid, P.G., 1989. Subendocardial infarction produces epicardial parasympathetic denervation in canine left ventricle. American Journal of Physiology. Heart and Circulatory Physiology 256, H859–H866.

Maughan, W.L., Sunagawa, K., Burkhoff, D., Graves, W.L. Jr., Hunter, W.C., Sagawa, K., 1985. Effect of heart rate on the canine end-systolic pressure–volume relationship. Circulation 72, 654–659.

Meisner, J.S., McQueen, D.M., Ishida, Y., Vetter, H.O., Bortolotti, U., Strom, J.A., Frater, R.W.M., Peskin, C.S., Yellin, E.L., 1985. Effects of timing of atrial systole on LV filling and mitral valve closure: computer and dog studies. American Journal of Physiology. Heart and Circulatory Physiology 249, H604–H619.

Mohrman, D.E., Heller, L.J., 1997. Cardiovascular Physiology, 4th ed. McGraw-Hill, New York, pp. 47–69.

Nakayama, Y., Miyano, H., Shishido, T., Inagaki, M., Kawada, T., Sugimachi, M., Sunagawa, K., 2001. Heart rate-independent vagal effect on end-systolic elastance of the canine left ventricule under various levels of sympathetic tone. Circulation 104, 2277–2279.

Przyklenk, K., Kloner, R.A., 1995. Low-dose i.v. acetylcholine acts as a "preconditioning-mimetic" in the canine model. Journal of Cardiac Surgery 10, 389–395.

Rosenshtraukh, L., Danilo Jr., P., Anyukhovsky, E.P., Steinberg, S.F., Rybin, V., Brittain-Valenti, K., Molina-Viamonte, V., Rosen, M.R., 1994. Mechanisms for vagal modulation of ventricular repolarization and of coronary occlusion-induced lethal arrhythmias in cats. Circulation Research 75, 722–732.

Schömig, A., Fischer, S., Kurz, T., Richardt, G., Schömig, E., 1987. Nonexocytotic release of endogenous noradrenaline in the ischemic and anoxic rat heart: mechanism and metabolic requirements. Circulation Research 60, 194–205.

Schwartz, J.H., 2000. Neurotransmitters. In: Kandel, E.R., Schwartz, J.H., Jessell, T.M. (Eds.), Principles of Neural Science, 4th ed. McGraw-Hill, New York, pp. 280–297.

Snedecor, G.W., Cochran, W.G., 1989. Statistical Methods, 8th ed. Iowa State, Iowa, pp. 290–291.

Suga, H., Hisano, R., Goto, Y., Yamada, O., Igarashi, Y., 1983. Effect of positive inotropic agents on the relation between oxygen consumption and systolic pressure volume area in canine left ventricle. Circulation Research 53, 306–318.

Vanoli, E., De Ferrari, G.M., Stramba-Badiale, M., Hull Jr., S.S., Foreman, R.D., Schwartz, P.J., 1991. Vagal stimulation and prevention of sudden death in conscious dogs with a healed myocardial infarction. Circulation Research 68, 1471–1481.

Yamazaki, T., Akiyama, T., Kitagawa, H., Takauchi, Y., Kawada, T., Sunagawa, K., 1997. A new, concise dialysis approach to assessment of cardiac sympathetic nerve terminal abnormalities. American Journal of Physiology. Heart and Circulatory Physiology 272, H1182–H1187.

Yamazaki, T., Akiyama, T., Mori, H., 2001. Effects of nociceptin on cardiac norepinephrine and acetylcholine release evoked by ouabain. Brain Research 904, 153–156.

Summary: An amphiphilic poly(*N*-propargylamide) with galactose and lauryloyl groups was synthesized by copolymerization of the corresponding *N*-propargylamide monomers using a Rh catalyst. The obtained copolymer formed a one-handed helical conformation and molecular aggregates in water. The observations by fluorescence microscopy in a cell culture experiment in the presence of dye-labeled copolymer indicated that the copolymer was incorporated into the cells.

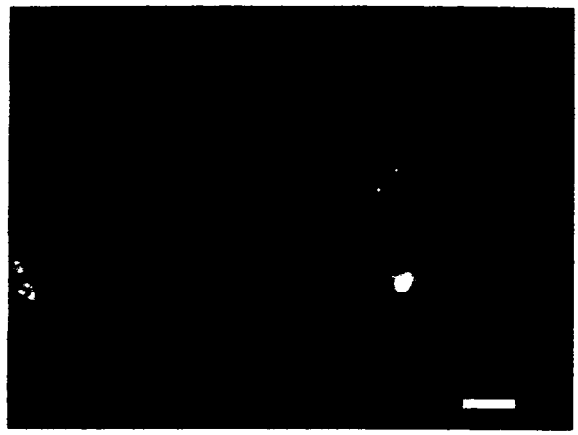

Localization of rhodamine B-labeled copolymer **8** in human aortic endothelial cells (fluorescence image).

Amphiphilic Poly(*N*-propargylamide) with Galactose and Lauryloyl Groups: Synthesis and Properties

Masakazu Suenaga,[1] *Yoshiro Kaneko,*[1] *Jun-ichi Kadokawa,**[1] *Takehiro Nishikawa,*[2] *Hidezo Mori,*[2] *Masayoshi Tabata*[3]

[1]Department of Nanostructured and Advanced Materials, Graduate School of Science and Engineering, Kagoshima 890-0065, Japan
Fax: +81-99-285-3253; E-mail: kadokawa@eng.kagoshima-u.ac.jp
[2]National Cardiovascular Center, Suita, Osaka 565-8565, Japan
[3]Department of Molecular Chemistry, Graduate School of Engineering, Hokkaido University, Sapporo 060-8628, Japan

Received: July 19, 2006; Accepted: October 10, 2006; DOI: 10.1002/mabi.200600228

Keywords: amphiphiles; conjugated polymers; copolymerization; dynamic light scattering; nanoparticles; polyacetylenes

Introduction

Synthesis of polymers having sugar residues, so-called glycopolymers, has been widely investigated to seek biological applications because of their versatile functions.[1] It has been demonstrated that these glycopolymers can bind specifically to carbohydrate-recognition proteins, toxins, viruses, and cells, and, thus, these polymers can be utilized as cell culture substrates with specific cell recognition sites, as well as in targeting drug delivery systems.[2] The clustered saccharide ligands conjugated to the polymeric main chains are involved in these specific recognition processes. Most of the previously prepared glycopolymers have been based on a flexible polymer backbone, such as polystyrene and polyacrylamide.[3,4] This flexible nature of the glycopolymers causes the disordered orientation of the sugar residues in the glycopolymers. Regular orientation of the sugar residues is necessary for efficient interaction between the glycopolymers and receptor molecules. In this sense, the spatially regulated orientation of the sugar residues should be realized by attaching the sugar residues to a polymer backbone with a rigid conformation. The sugar residues attached to the rigid polymer backbone may give rise to the ordered orientation that can improve the molecular recognition of sugar residues by specific cell receptors. This is because the spatial regulation of the sugar residues is significant in molecular recognition as well as the chemical structure of the sugar molecules.[5]

From the above viewpoints, rigid glycopolymers with π-conjugated polymer backbones would be a novel type of bio-inspired polymers, which could exhibit multiple valence states and interact specifically and firmly with targets such as cell surface receptors and biomacromolecules. In some previous works, rigid glycopolymers having various π-conjugated main chains, such as polythiophene,[6] poly(*p*-phenylene ethynylene),[7] polyisocyanide,[8] polyaniline,[9] poly(*p*-phenylene vinylene),[10] and poly(phenylacetylene), have already been synthesized.[11] In the series of these studies, we reported the synthesis of poly(*N*-propargylamide) (**2**) with sugar residues. It contained a *cis*-polyacetylene main chain and was obtained by the rhodium-catalyzed polymerization of a *N*-propargylamide monomer (**1**) that had a galactose residue (Scheme 1).[12] Since polymerizations of the *N*-propargylamide monomers having various substituted groups using Rh catalyst have been widely reported to produce the corresponding poly(*N*-propargylamide) derivatives with *cis*-isomers,[13] we also investigated the copolymerization of **1** with *N*-propargylamide derivative **3** having a hexanoyl group to produce the amphiphilic glycopolymer **4**, as shown in Scheme 1. We tested the solubility of copolymer **4** in various solvents to confirm whether the copolymer exhibits an amphiphilic property. Although the homopolymer **2** is insoluble in common organic solvents, the copolymer **4** can be dissolved in some polar organic solvents, such as dimethyl sulfoxide (DMSO) and *N,N*-dimethylformamide (DMF), as well as in aqueous medium. However, the copolymer still exhibits a hydrophilic nature rather than an amphiphilic nature. We assumed that insufficient amphiphilicity of copolymer **4** could be attributed to poor hydrophobic property of the hydrophobic part.

In this study, we chose a more hydrophobic monomer; *N*-propargylamide monomer **5** having a longer alkyl chain, i.e., the lauryloyl group, as the hydrophobic part of the amphiphilic copolymer. The monomer **5** was copolymerized with **1** in the presence of Rh catalyst to give the corresponding amphiphilic copolymer **6** (Scheme 2). The resulting copolymer **6** can be expected to have the ability to conduct molecular aggregation in water, which is driven by intermolecular and intramolecular association of the hydrophobic lauryloyl groups.

We believe that such molecular aggregates of the amphiphilic copolymer should play a significant role in the field of targeted drug delivery. The idea is supported by the following characteristics of the molecular aggregates:

1) Drug carriers with nanometer dimensions can be obtained by molecular aggregation of amphiphilic copolymers.
2) Nano-sized aggregates can remain in the bloodstream for an extended period because of the size-dependent uptake in the reticuloendothelial system.
3) Drug molecules with hydrophobic natures can be loaded into hydrophobic milieus formed by the association of hydrophobic long alkyl chains; otherwise the drug molecules could be directly attached to the constituent monomer molecules of the copolymer.
4) Sugar residues of the copolymer can function as recognition sites for target cells and tissues as well as providing the hydrophilic character of the amphiphilic copolymer.

Therefore, we studied the *in vitro* cell uptake of the molecular aggregates of the amphiphilic copolymer. For this purpose, the fluorescent marker, rhodamine B, was introduced into the amphiphilic copolymer. In this article, we report the synthesis of the amphiphilic

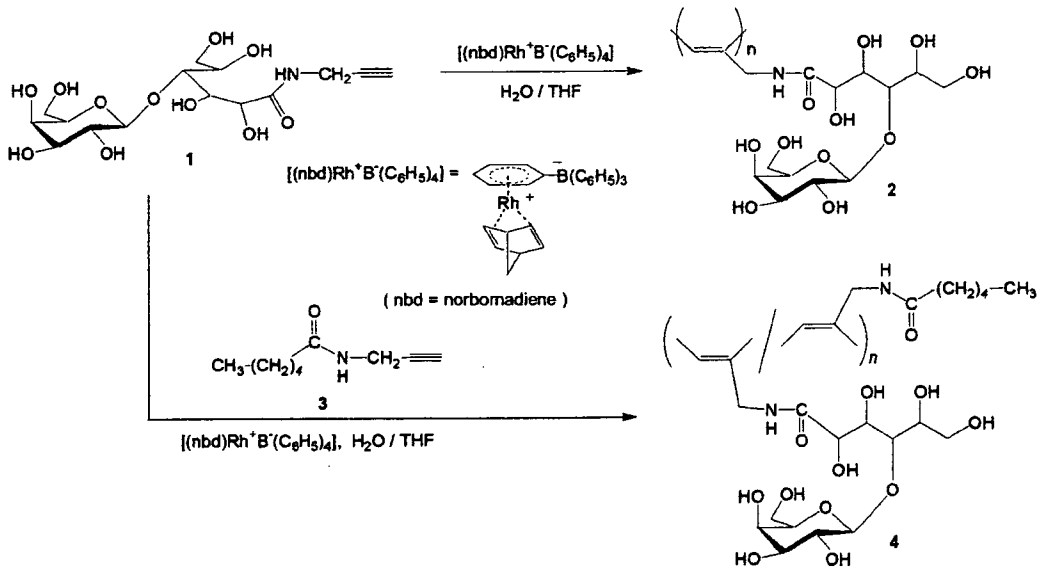

Scheme 1. Polymerization of **1** and copolymerization of **1** with **3**.

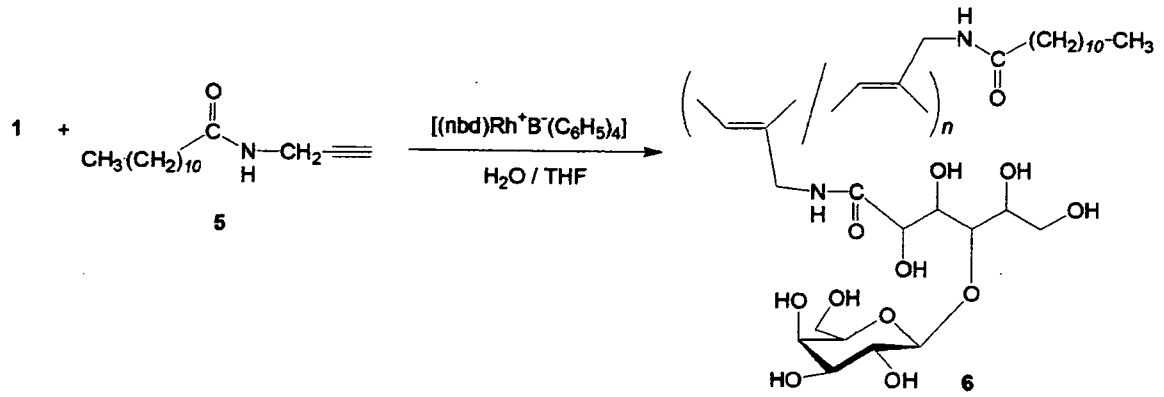

Scheme 2. Copolymerization of **1** with **5**.

poly(*N*-propargylamide) **6** by Rh-catalyzed copolymerization, evaluation of its molecular aggregation in water [gel permeation chromatography (GPC) characterization, scanning electron microscopy (SEM) observation, and dynamic light scattering (DLS) measurement] and secondary conformation [circular dichroism (CD) spectra], and cell uptake of the nanoaggregate of the rhodamine-labeled amphiphilic copolymer (fluorescence microscopy).

Experimental Part

Materials

Monomer **1** and catalyst (nbd)$Rh^+B^-(C_6H_5)_4$ were prepared according to the literature.[12,14] Tetrahydrofuran (THF) used as polymerization solvent was purified by distillation. Other reagents and solvents were used as received without further purification.

Synthesis of Monomer 5

Monomer **5** was synthesized by a method similar to that used for **3**.[15] Under argon, *N*-propargylamine hydrochloride (0.915 g, 10.0 mmol) was dissolved by slight warming in anhydrous acetonitrile (12.0 mL), and triethylamine (3.35 mL, 24.0 mmol) was added to the solution at room temperature. Then a solution of lauryloyl chloride (2.36 mL, 10.0 mmol) in anhydrous acetonitrile (12.0 mL) was added dropwise to the solution. After the mixture was stirred for 2 h, the reaction solution was concentrated by evaporation. The residue was dissolved in ethyl acetate and the solution was washed successively three times with 2 mol·L^{-1} hydrochloric acid and with saturated $NaHCO_3$ aqueous solution. The organic layer was dried over anhydrous Na_2SO_4, filtered, and evaporated. The residue was subjected to column chromatography on silica gel (hexane:ethyl acetate = 4:1, v/v) to isolate **5** (1.38 g, 5.82 mmol) in 58.2% yield.

^{1}H NMR ($CDCl_3$): $\delta = 0.88$ (t, $J = 7.2$ Hz, CH_3, 3H), 1.28 [m, $CH_3(CH_2)_8$, 16H], 1.62 (m, $CH_2CH_2C{=}O$, 2H), 2.19 (t, $J = 7.8$ Hz, $CH_2C{=}O$, 2H), 2.23 (t, $J = 2.4$ Hz, H–C≡C, 1H), 4.05–4.06 (m, CH_2N, 2H), 5.57 (s, NH, 1H).

Synthesis of Monomer 7

Under argon, triethylamine (0.836 mL, 6.00 mmol) was added to a solution of *N*-propargylamine hydrochloride (0.549 g, 6.00 mmol) and rhodamine B (1.92 g, 4.0 mmol) in anhydrous methanol (10.0 mL) at 0 °C. To the solution was added 1-[(3-dimethylamino)propyl]-3-ethylcarbodiimide hydrochloride (1.15 g, 6.00 mmol) as a condensing agent at 0 °C and the mixture was stirred for 17 h at room temperature. The precipitated material was isolated by filtration and dried under the reduced pressure to give **7** (0.472 g, 0.915 mmol) in 23.0% yield.

^{1}H NMR ($CDCl_3$): $\delta = 1.16$ (m, CH_3, 12H), 1.77 (t, $J =$ 2.4 Hz, H–C≡C, 1H), 3.33 (m, NCH_2CH_3, 8H), 3.95 (d, $J = 1.8$ Hz, $CH_2C{\equiv}$, 2H), 6.26–7.93 (m, aromatics, 10H).

Copolymerization of 1 with 5

A typical copolymerization procedure was as follows (entry 1, Table 1). Under argon, a solution of **5** (0.0356 g, 0.150 mmol) in THF (0.90 mL) and a solution of catalyst (0.00630 g, 0.0125 mmol) in THF (0.90 mL) were added to a solution of **1** (0.0397 g, 0.100 mmol) in water (0.20 mL) in this order at 30 °C. After the mixture was stirred at 30 °C for 140 min, the reaction mixture was concentrated by evaporation and dried under reduced pressure. The residue was dissolved in a small amount of DMSO and the solution was poured into a large amount of methanol to precipitate the polymeric product. The precipitate was isolated by filtration and was dried under reduced pressure to give **6** (0.0588 g) in 78.1% yield.

^{1}H NMR (DMSO-d_6): $\delta = 0.84$ (CH_3), 1.21 [$CH_3(CH_2)_8$], 1.45 ($CH_2CH_2C{=}O$), 2.15 ($CH_2C{=}O$), 3.0–3.9 [–CH(O-D-gal)–CH(OH)–CH_2OH, $=CCH_2-$, H2–H6 of D-gal], 4.04 [C(=O)CH(OH)CH(OH)–], 4.29 [C(=O)CH(OH)– and H1(β) of D-gal], 4.55, 4.79, 5.22 (OH), 6.11 (–CH=C–), 7.93 (NH).

Copolymerization of 1, 5, and 7

Under argon, a solution of **5** (0.0285 g, 0.120 mmol) and **7** (0.0929 g, 0.180 mmol) in THF (0.90 mL) and a solution of catalyst (0.0166 g, 0.0330 mmol) in THF (0.90 mL) were

Table 1. Results for copolymerization of **1** with **5** with Rh catalyst in THF–water (9:1) solvent.

Entry	Feed ratio[a]	Time	Yield[b]	Unit ratio[c]	$\overline{M}_n$[d]	$\overline{M}_w/\overline{M}_n$[d]	$[\alpha]_D$[e]
	1:5	min	%	1:5			degrees
1	1.0:1.5	140	78.1	1.0:0.92	9100	1.30	–
2	1.0:1.0	195	62.5	1.0:0.88	6200	1.63	–
3	1.0:0.67	240	57.0	1.0:0.35	5200	1.60	+96.8
4	1.0:0.50	260	68.9	1.0:0.32	9600	1.64	+142.3
5	1.0:0.33	200	69.9	1.0:0.26	7100	1.50	+173.6
6	1.0:0.20	210	78.1	1.0:0.17	9700	1.30	+185.6

[a] [Catalyst]/[1 + 5] = 0.05, reaction temperature; 30 °C.
[b] Fraction insoluble in methanol.
[c] Determined from ^{1}H NMR spectra.
[d] Determined by GPC with water as eluent using pullulan standards, sample concentration = 0.1 mg · mL^{-1}.
[e] Measured by polarimetry in water, c = 1.0 g · dL^{-1} at 20 °C.

added to a solution of **1** (0.143 g, 0.360 mmol) in water (0.20 mL) in this order at 30 °C. After the mixture was stirred at 30 °C for 18 h, the reaction mixture was concentrated by evaporation and dried under reduced pressure. The residue was dissolved in a small amount of DMSO and the solution was poured into a large amount of methanol to precipitate the polymeric product. The precipitate was isolated by filtration and dried under reduced pressure to give **8** (0.164 g) in 62.0% yield.

^{1}H NMR (DMSO-d_6 + D_2O): δ = 0.93 ($CH_3CH_2CH_2$), 1.16 (CH_3CH_2N), 1.25 [$CH_3(CH_2)_8$], 1.50 ($CH_2CH_2C{=}O$), 3.0–4.5 (sugar protons and =C–CH_2), 6.16 (HC=), 7.0–8.0 (aromatics).

Cell Culture Experiment

Human aortic endothelial cells (HAECs) were purchased as cryopreserved samples of third passage (Lot: 3F1346) from Cambrex (Wakersville, MD, USA). The HAECs were subcultured once and stored in liquid nitrogen until cell culture experiment. The HAECs used in the experiment were fourth passage. Each well of a 12-well plate of polystyrene (Iwaki) was filled with 1 mL of a supplemented culture medium (EGM-2; Lot: 08103123, Cambrex) and equilibrated at 37 °C in a humidified incubator under 5% CO_2 for 30 min before cell seeding. After the frozen cells were thawed at 37 °C, 10 μL of the cell suspension was seeded in each well. The initial cell density was 2.2×10^3 cells · cm^{-2}. Cell viability assessed by the trypan blue exclusion test was 83% for the cell suspension. The cell seeded plates were placed in a humidified incubator at 37 °C under 5% CO_2. The HAECs were cultured for 48 h. Cell culture mediums were replaced with fresh medium 24 h after cell seeding. At 48 h after cell seeding, cell culture mediums were each replaced with an aqueous suspension of copolymer **8**. Then the HAECs were cultured in the polymer suspension for 1, 6, and 24 h in a humidified incubator at 37 °C under 5% CO_2 to study cellular uptake of nanoaggregates of copolymer **8**. For fluorescence microscopy observation, the cells were fixed by immersion in 10% formaldehyde neutral buffer solution (Nacalai Tesque) at room temperature (22 °C) for 15 min and were washed three times with phosphate-buffered saline (PBS; Gibco). Fluorescence images of the cells were taken with a fluorescence microscope (IX71; Olympus) equipped with a CCD camera (DP70; Olympus). Fluorescence intensity of the incorporated copolymer **8** was measured by integrating the fluorescence intensity observed at each pixel of the fluorescence images using image analysis software (Fluoview ver. 5.0; Olympus).

Measurements

NMR spectra were recorded on a JEOL ECA 600 spectrometer. Optical rotations were measured with a Jasco P-1030 digital polarimeter. GPC analyses were performed by using a TOSOH 8012 with refractive index detection under the following conditions: Shodex Asahipak GF-310HQ column with water as eluent at a flow rate of 0.5 mL · min^{-1}. The calibration curve was obtained using pullulan standards. CD and UV-vis spectra were measured in a quartz cell (thickness 1 cm) at room temperature using a Jasco J-820 spectropolarimeter and Shimadzu UV160A spectrophotometer, respectively. The SEM images were obtained using a Hitachi S-4100 electron microscope. The DLS measurement was performed on a Zetasizer 3000 (Malvern Instruments). Fluorescence spectra were obtained on a fluorescence spectrometer (Shimadzu) using a quartz cuvette (1-mm path length).

Results and Discussion

Copolymerization of 1 with 5

The polymerization of monosubstituted acetylene derivatives has been widely investigated using Rh complex catalysts, which enables stereoselective synthesis of the corresponding polyacetylenes of the *cis*-isomers.[16] As

already reported in our previous publication, **1** was polymerized using (nbd)$Rh^+B^-(C_6H_5)_4$ as the catalyst at around 25° to 50 °C in a mixed solvent of THF and water (9:1, v/v).[12] In this study, we performed the copolymerization of **1** with **5** under similar conditions. The copolymerization with various feed ratios of **1** to **5** was carried out using the Rh catalyst (5.0 mol-% for **1** + **5**) at 30 °C in a THF-water mixed solvent under argon. After polymerization, the resulting mixture was concentrated and then dissolved in DMSO. The solution was poured into a large amount of methanol to precipitate the polymeric product. The precipitate was isolated by filtration and dried under reduced pressure to give the copolymer **6** (Table 1). The copolymer was soluble in water and DMSO, and its $\overline{M}_n$ value was estimated by GPC analysis with water as eluent using pullulan standards. Figure 1a shows the ^{1}H NMR spectrum of the copolymer (entry 1, Table 1) measured in DMSO-d_6. The signals due to the sugar and alkyl protons are observed at around δ 3.0–4.3 (signals **e–h**) and δ 0.84, 1.21, 1.45, 2.15 (signals **a–d**), respectively. In addition to these signals, signal **i** ascribed to the main-chain proton of –CH=C– appears centered at δ 6.11. The chemical shift of this signal realistically corresponds to the *cis*-isomer. Furthermore, there is no signal due to the *trans*-isomer at lower magnetic field from the *cis*-signal. The NMR results support structure **6** as that of the copolymer, which is mainly composed of *cis*-isomer. The unit ratio of the copolymer is calculated by the integrated ratio of signal **a** and signal **i**.

Table 1 shows the copolymerization results obtained by the various feed ratios of **1** to **5**. The yields and the $\overline{M}_n$ values are 57.0–78.1% and 5 200–9 700, respectively. The unit ratios of **5** in the copolymers increase with increasing molar ratios of **5** in the feeds. In all cases, however, the ratios of **5** in the copolymers are lower than those in the feeds. This is probably because the copolymers with higher

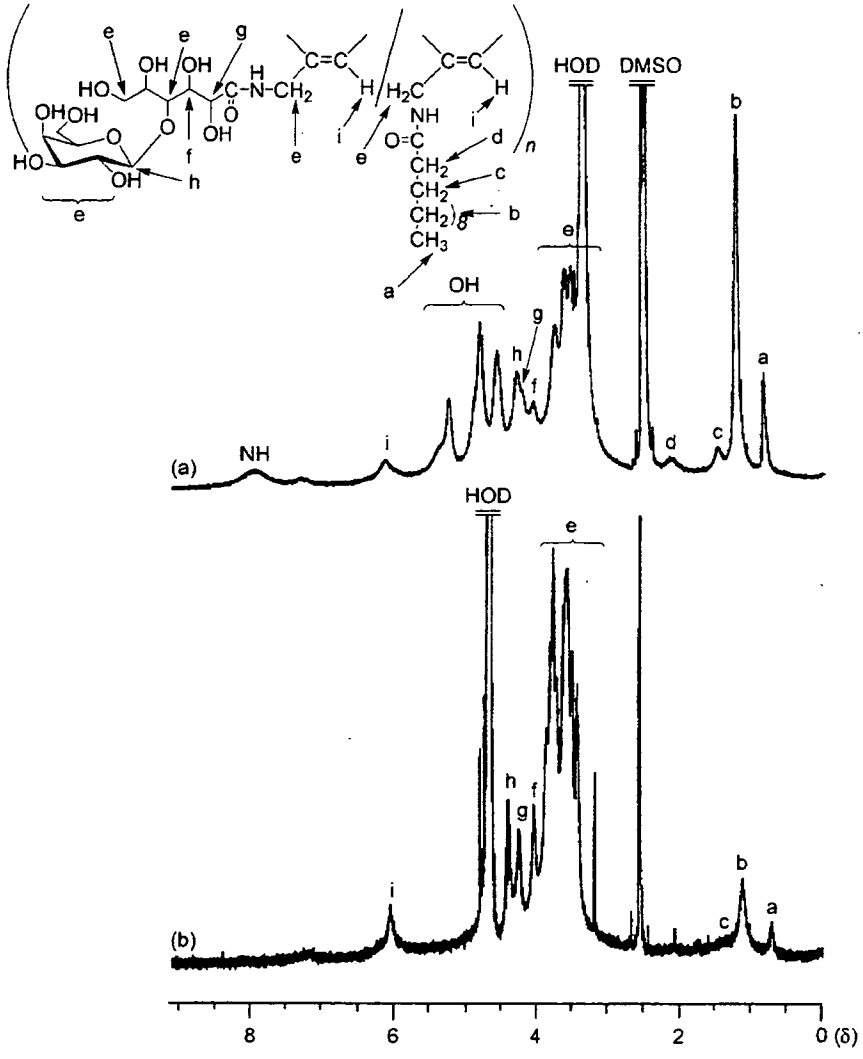

Figure 1. ^{1}H NMR spectra of copolymer **6** (entry 1, Table 1) in DMSO-d_6 (a) and D_2O (b).

contents of the unit **5** are lost as methanol-soluble fractions during the isolation procedure. The optical rotations of the copolymers with the higher contents of the sugar units were larger than those with the lower contents.

Formation of Molecular Aggregates in Water

When the copolymerization was followed by thin-layer chromatography (TLC) on silica gel (methanol: chloroform = 2:1 for **1**; hexane: ethyl acetate = 1: 1 for **5**), **1** appeared to be consumed at the early stage of the reaction; subsequently, the consumption of **3** at a later stage was confirmed. This indicated that **6** had the block copolymeric sequence between the unit **1** and the unit **5** rather than in random style. In fact, the intensities of the alkyl signals **a–d** in the ^{1}H NMR spectrum of **6** in D_2O (Figure 1b) are obviously lower than those of the same copolymer measured in DMSO-d_6 (Figure 1a). The NMR results suggest formation of micelle-like aggregates having the outer hydrophilic sugar residues and the inner hydrophobic lauryloyl groups in water, and this was attributed to the block copolymeric sequence. The formation of molecular aggregates of **6** in water was also confirmed by the GPC measurements on aqueous solutions of **6** (entry 5, Table 1, the unit ratio of **1** to **5** = 1.0:0.26) ranging in concentration from 0.05 to 9.0 mg · mL^{-1}. Figure 2 shows the relations of the $\overline{M}_n$ values to the sample concentrations in the GPC experiments. The $\overline{M}_n$ values increase from ca. 6300 to ca. 11000 for concentrations higher than 0.70 mg · mL^{-}. These data suggest the formation of molecular aggregates for the higher concentrations of **6** in water. The molecular aggregates of **6** were directly observed by SEM. The SEM image of the spin-coated sample from the aqueous solution of **6** (entry 4, Table 1, the unit ratio of **1** to **5** = 1.0:0.32) on aluminium plate (Figure 3) shows the particle-type molecular aggregates with average diameters of 20–40 nm. The particle sizes were also confirmed by DLS measurement. The mean particle diameter of the sample shown as entry 4 in Table 1 was 85.2 ± 14.1 nm. The difference in the aggregate sizes obtained by SEM and DLS can be attributed to the difference in the sample condition: dry for SEM and wet for DLS.

Secondary Conformation of 6

We already reported in our previous report that the CD spectrum of the homopolymer **2** in water showed the positive Cotton effect at 330 nm corresponding to the main-chain UV-vis absorption.[12] This indicated the possibility for formation of a one-handed helical conformation in the main chain of **2**. In this study, the CD analysis was also performed to reveal the secondary conformation of copolymer **6**. Figure 4 shows the CD spectra of **6** (entry 5, Table 1, unit ratio of **1** to **5** = 1.0:0.26) in comparison with those of copolymer **4** (unit ratio of **1** to **3** = 1.0: 0.39) measured in DMSO and water at room temperature. The CD spectrum of **6** in DMSO (Figure 4a) shows the positive Cotton effect at 360 nm, corresponding to the main-chain UV-vis absorption. The positive Cotton effect also appeared at this region in the CD spectrum in water (Figure 4b), although its intensity was lower than that in DMSO. It has been reported that the helical structure of poly(*N*-propargylamide)s is stabilized by the intramolecular hydrogen bonds between the pendant amide groups.[17] In polar solvents such as DMSO and water, therefore, the hydrogen bonds are readily broken to effect destabilization of the helical structure. The helical conformation of **6** in polar solvents is probably stabilized by the bulky substituents in the side chains of sugar and lauryloyl groups. These bulky groups shield the hydrogen bonds from the solvents, which consequently stabilizes the helical structure. This reasoning is also supported by comparison of the CD spectra of copolymer **4** (gray lines in

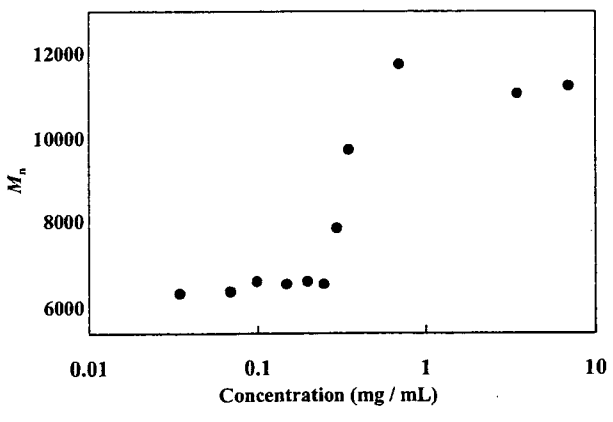

Figure 2. $\overline{M}_n$ values versus sample concentrations in GPC measurements with water as eluent (entry 5, Table 1).

Figure 3. SEM image of **6**; the sample was prepared by spin coating of the dispersed solution of **6** (entry 4, Table 1) in water.

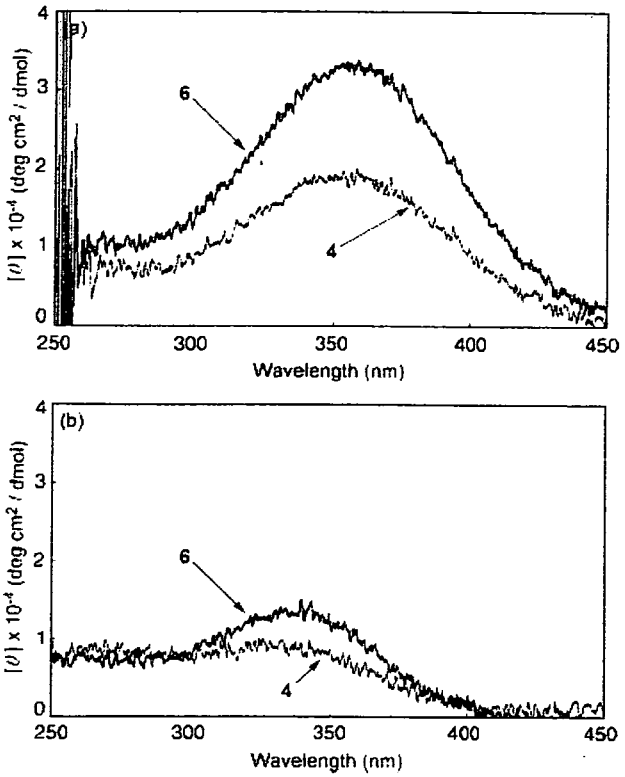

Figure 4. CD spectra of **6** (entry 5, Table 1, unit ratio; 1:5 = 1.0:0.26) and **4** (unit ratio; 1:3 = 1.0:0.39) in DMSO (a) and water (b) ($c = 0.2$ mmol · L^{-1}).

Figure 4a, b), which has the less bulky hexanoyl groups. The CD spectra of **4** show weaker Cotton effects than those of **6**, indicating the stabilization of the helical conformation as a result of the bulkiness of the pendant groups.

Cellular Uptake of Amphiphilic Copolymer 8

To evaluate cell uptake of the copolymer by fluorescence microscopy, the rhodamine B dye moiety was introduced into the amphiphilic copolymer. First, an *N*-propargylamide derivative **7** having a pendant rhodamine B moiety was prepared by condensation of *N*-propargylamine hydrochloride with rhodamine B in the presence of a condensing agent (1-[(3-dimethylamino)propyl]-3-ethylcarbodiimide hydrochloride) in methanol. Then, the isolated **7** was copolymerized with **1** and **5** under conditions similar to those described above (Scheme 3). Although **7** did not have homopolymerizability by Rh catalyst, the unit from **7** was slightly incorporated into the resulting terpolymer by the copolymerization. The existence of the rhodamine B moiety in the obtained terpolymer **8** was confirmed by appearance of the signals due to methyl protons of N-CH_2CH_3 as well as the aromatic protons in the ^{1}H NMR spectrum of the product. However, the intensities of the signals were too weak to determine the exact content of the dye moiety in the copolymer by the integration ratio. For comparison, hydrophilic copolymer **9** was synthesized by copolymerization of monomer **1** with monomer **7** using Rh catalyst (Figure 5).

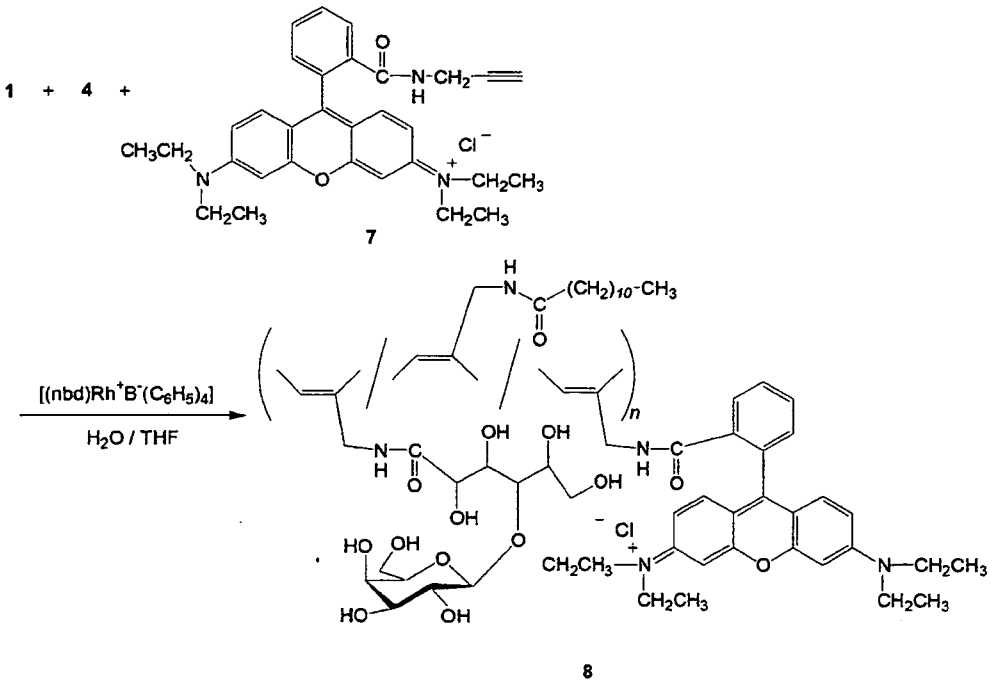

Scheme 3. Terpolymerization of **1**, **5**, and **7**.

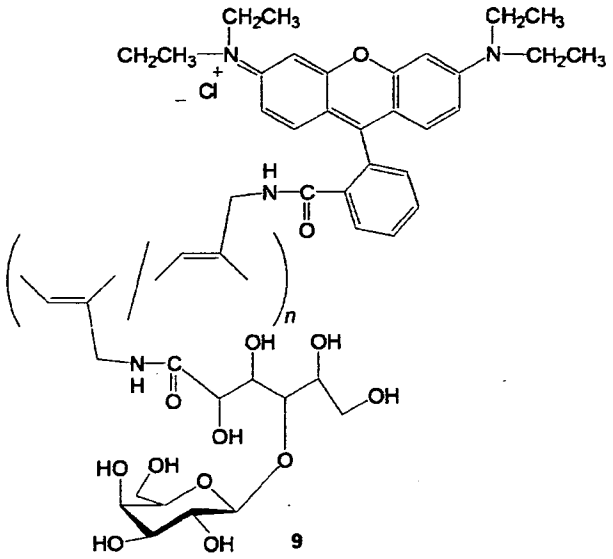

Figure 5. Structure of copolymer **9**.

The cell uptake of terpolymer **8** was studied by culturing human aortic endothelial cells (HAECs) in a culture medium containing the terpolymer **8**. Ten milligrams of **8** was suspended in 10 mL of culture medium EGM-2 and stirred for 3 h at room temperature. The suspension of **8** was sonicated at 25 W and 40 kHz for 5 min in an ultrasonic bath. The sonication was repeated twice. The obtained suspension was filtered through membrane filters with the pore sizes of 0.45 μm and 0.2 μm for sterilization. An aqueous solution of polymer **9** was prepared by following the above procedure. To evaluate the concentration of **8**, a calibration curve (data not shown) was obtained by using the aqueous solution of **9** (1 mg · mL^{-1}) as a standard polymer sample to relate concentration to fluorescence intensity. The concentration of **8** was estimated to be 0.09 mg · mL^{-1} by using the calibration curve. The DLS measurement revealed that the polymer aggregates (nanoparticles) of **8** have a mean diameter of 114.9 ± 32 nm in a culture medium containing 10% bovine serum. HAECs were exposed to the polymer aggregates of **8** while they were cultured in the culture medium containing the amphiphilic polymer **8**. After the prescribed period of culture, 1, 6, or 24 h, the HAECs were fixed in 10% formaldehyde neutral buffer solution for microscope observation. Figure 6 shows phase contrast (a), fluorescence (b), and merged (phase contrast + fluorescence) (c) images of HAECs after 24 h of incubation. The merged image demonstrates that red fluorescent light of rhodamine B was emitted from the sites where HAECs were located. This indicates that the polymer aggregates of **8** were incorporated into HAECs. The fluorescence images at each time of incubation are shown in Figure 7. The fluorescence images get brighter with the incubation time. To quantitatively evaluate cell uptake of nanoaggregates, fluorescence intensity per image (1 360 × 1 024 pixels) was determined by integrating the brightness at each pixel of the fluorescence image using image analysis software. The

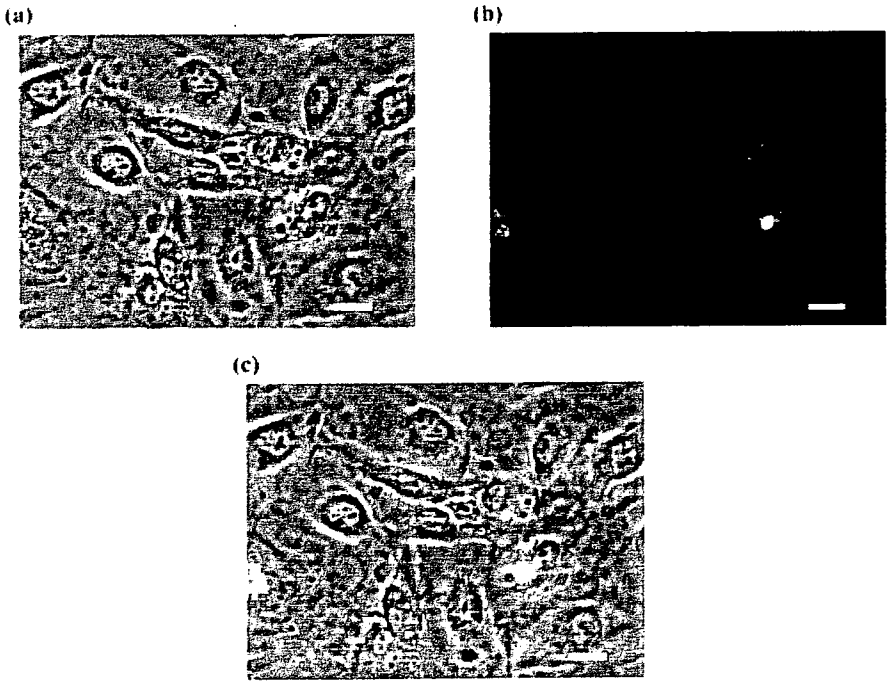

Figure 6a–c.. Localization of rhodamine B-labeled copolymer **8** in human aortic endothelial cells. Phase contrast image (a), fluorescence image (b), and merged image of (a) and (b). Bars: 20 μm.

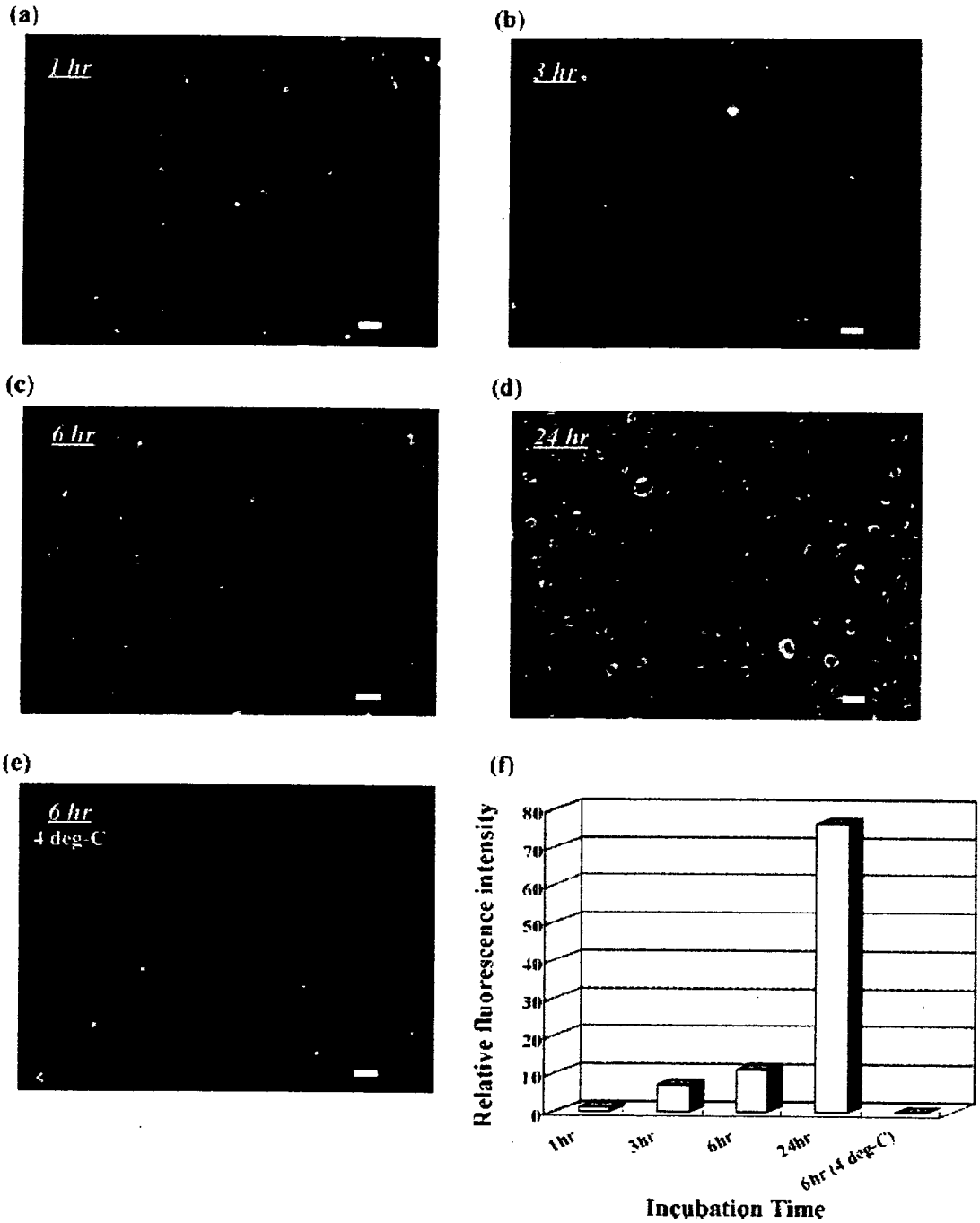

Figure 7a–f. Uptake of rhodamine B-labeled copolymer **8** by human aortic endothelial cells; incubation time, 1 h (a), 3 h (b), 6 h (c), 24 h (d) (incubation at 37 °C), and 6 h (incubation at 4 °C) (e). Bars: 20 μm. The uptake is quantitatively represented as relative fluorescence intensity in the bar graph (f).

fluorescence intensity was normalized in a ratio of the fluorescence intensity at each incubation time to that at 1 h of incubation. The ratio was termed as the relative fluorescence intensity. The time course of the relative fluorescence intensity is shown in Figure 7f and indicates that HAECs incorporated progressively more nanoaggregates of **8** during the incubation time. The relative fluorescence intensity was 7-fold at 3 h, 11-fold at 6 h, and 76-fold at 24 h of incubation. In contrast, the relative fluorescence intensity dropped considerably and was only 12% of the control level (1 h at 37 °C) when HAECs were exposed to the nanoaggregates of **8** at 4 °C for 6 h. The fact that the temperature triggered a dramatic decrease in the relative fluorescence intensity suggests that the nanoag-

gregates are incorporated into HAECs by endocytosis. Endocytosis is known as a cellular process that is coupled with temperature-dependent metabolic activities.[18] Furthermore, it is known that some receptors and membrane microdomains of endothelial cell are involved in endocytosis.[19] However, it is not clear which of the endocytic pathways is responsible for the uptake of the nanoaggregates. This issue is now under investigation.

Conclusion

In this study, we investigated synthesis of the amphiphilic poly(*N*-propargylamide) **6** containing both sugar residues (hydrophilic part) and long alkyl chains (hydrophobic part) in order to develop a novel nanoaggregate based on the self-organization of amphiphilic polymers with rigid backbone. The desired polymer was prepared by copolymerization of the two *N*-propargylamide monomers **1** and **5** having a galactose residue and a lauryloyl group, respectively, catalyzed by a Rh complex. The GPC, ^{1}H NMR, SEM, and DLS analyses of the resulting copolymers indicated formation of the nanoparticles in water. The formation of the one-handed helical conformation of the copolymer in both DMSO and water was confirmed by the CD spectra. An amphiphilic poly(*N*-propargylamide) containing fluorescent dyes was newly designed to evaluate cell uptake of nanoparticles of the amphiphilic copolymer by fluorescence microscopy. The *N*-propargylamide monomer **7**, having a rhodamine B dye moiety, was prepared and copolymerized with **1** and **5**. Human aortic endothelial cells (HAECs) were cultured in a medium containing the fluorescent-dye-labeled amphiphilic copolymer. Cell uptake of the copolymer was confirmed by red fluorescence emission from each of the HAECs. Progressive uptake was observed during the incubation period. When the cell culture experiment was conducted at 4 °C, the fluorescence intensity of the red emission was considerably lowered. This indicates that the cell uptake is inhibited at 4 °C and that this uptake process should occur in an endocytic pathway rather than by simple adsorption to the plasma membrane of HAECs. We are now synthesizing a fluorescent-dye-labeled hydrophilic copolymer of monomer **1** with monomer **7** to study preferential cell uptake of the nanoaggregates of the amphiphilic copolymer. In the future, we anticipate that nanoparticles will be able to be preferentially endocytosed into cells rather than monomeric chains of water-soluble copolymer. If this does occur, the nanoparticles of the amphiphilic copolymer will be a promising nanocarrier for drug delivery.

Acknowledgements: This work was financially supported by the *Asahi Glass Foundation*. The author (T. N.) thanks Professor *Mitsuru Akashi* of Osaka University and Dr. *Takami Akagi* of the Japan Science and Technology Agency for dynamic light scattering measurement. The author (T. N.) thanks Dr. *Tetsuji Yamaoka* and Dr. *Atsushi Mahara* of the National Cardiovascular Center Research Institute for fluorescence spectroscopy analysis.

[1] M. Okada, *Prog. Polym. Sci.* **2001**, *26*, 67.
[2] Y. C. Lee, R. T. Lee, " *Neoglycoconjugates: Preparation and Applications*", Academic Press, San Diego **1994.**
[3] K. Kobayashi, A. Tsuchida, T. Usui, T. Akaike, *Macromolecules* **1997**, *30*, 2016.
[4] K. Kobayashi, N. Kakishita, M. Okada, T. Akaike, T. Usui, *J. Carbohydr. Chem.* **1994**, *13*, 753.
[5] L. L. Kiessling, N. L. Pohl, *Chem. Biol.* **1996**, *3*, 71.
[6] M.-G. Baek, R. C. Stevens, D. H. Charych, *Bioconjugate Chem.* **2000**, *11*, 777.
[7] I.-B. Kim, B. Erdogan, J. N. Wilson, U. H. F. Bunz, *Chem. Eur. J.* **2004**, *10*, 6247.
[8] T. Hasegawa, S. Kondoh, K. Matsuura, K. Kobayashi, *Macromolecules* **1999**, *32*, 6595.
[9] J. Kadokawa, Y. Shinmen, S. Shoda, *Macromol. Rapid Commun.* **2005**, *26*, 103.
[10] A. Takasu, K. Iso, T. Dohmae, T. Hirabayashi, *Biomacromolecules* **2006**, *7*, 411.
[11] K. Matsuura, S. Furuno, K. Kobayashi, *Chem. Lett.* **1998, 847.**
[12] J. Kadokawa, K. Tawa, M. Suenaga, Y. Kaneko, M. Tabata, *J. Macromol. Sci., Pure Appl. Chem.* **2006**, *43*, 1179.
[13] J. Deng, J. Tabei, M. Shiotsuki, F. Sanda, T. Masuda, *Macromolecules* **2004**, *37*, 9715 and references therein.
[14] R. R. Shrock, J. A. Osborn, *Inorg. Chem.* **1970**, *9*, 2339.
[15] J. Deng, J. Tabei, M. Shiotsuki, F. Sanda, T. Masuda, *Macromolecules* **2004**, *37*, 1891.
[16] M. Tabata, T. Sone, Y. Sadahiro, *Macromol. Chem. Phys.* **1999**, *200*, 265.
[17] J. Tabei, R. Nomura, T. Masuda, *Macromolecules* **2002**, *35*, 5405.
[18] G. Durin, S. Cottin, E. Blanc, A. R. Rees, *J. Temsamani, J. Biol. Chem.* **2003**, *278*, 31192.
[19] S. Muro, M. Koval, V. Muzykantov, *Curr. Vasc. Pharmacol.* **2004**, *2*, 281.

nature medicine

Monolayered mesenchymal stem cells repair scarred myocardium after myocardial infarction

Yoshinori Miyahara[1,9], Noritoshi Nagaya[1,9], Masaharu Kataoka[1], Bobby Yanagawa[1], Koichi Tanaka[1], Hiroyuki Hao[2], Kozo Ishino[3], Hideyuki Ishida[4], Tatsuya Shimizu[5], Kenji Kangawa[6], Shunji Sano[3], Teruo Okano[5], Soichiro Kitamura[7] & Hidezo Mori[8]

Mesenchymal stem cells are multipotent cells that can differentiate into cardiomyocytes and vascular endothelial cells. Here we show, using cell sheet technology, that monolayered mesenchymal stem cells have multipotent and self-propagating properties after transplantation into infarcted rat hearts. We cultured adipose tissue–derived mesenchymal stem cells characterized by flow cytometry using temperature-responsive culture dishes. Four weeks after coronary ligation, we transplanted the monolayered mesenchymal stem cells onto the scarred myocardium. After transplantation, the engrafted sheet gradually grew to form a thick stratum that included newly formed vessels, undifferentiated cells and few cardiomyocytes. The mesenchymal stem cell sheet also acted through paracrine pathways to trigger angiogenesis. Unlike a fibroblast cell sheet, the monolayered mesenchymal stem cells reversed wall thinning in the scar area and improved cardiac function in rats with myocardial infarction. Thus, transplantation of monolayered mesenchymal stem cells may be a new therapeutic strategy for cardiac tissue regeneration.

Myocardial infarction, a main cause of heart failure, leads to loss of cardiac tissue and impairment of left ventricular function. Therefore, restoring the scarred myocardium is desirable for the treatment of heart failure. Although needle injections of bone marrow cells into the myocardium have been performed for cardiac regeneration[1–5], it is difficult to reconstruct sufficient cardiac mass in the thinned scar area after myocardial infarction.

Recently, our colleagues have developed cell sheets using temperature-responsive culture dishes[6]. These cell sheets allow for cell-to-cell connections and maintain the presence of adhesion proteins because enzymatic digestion is not needed[7–10]. Therefore, cell sheet transplantation may be a promising strategy for partial cardiac tissue reconstruction. Skeletal myoblasts, fetal cardiomyocytes and embryonic stem cells have been considered as candidates for an implantable cell source[11–13]. It is difficult, however, to produce a multilayered construct requiring a vascular network. Thus, autologous somatic stem cells with self-propagating properties that can induce angiogenesis are a desirable cell source for a transplantable sheet.

Mesenchymal stem cells (MSCs) are multipotent adult stem cells that reside within the bone marrow microenvironment[14,15]. MSCs can differentiate not only into osteoblasts, chondrocytes, neurons and skeletal muscle cells, but also into vascular endothelial cells[16] and cardiomyocytes[17–20]. In contrast to their hematopoietic counterparts, MSCs are adherent and can expand in culture. Recently, MSCs have been isolated from adipose tissue[21–24], which is typically abundant in individuals with cardiovascular disease. Here, we investigated the therapeutic potency of monolayered MSCs derived from adipose tissue using cell sheet technology.

RESULTS

Characteristics of adipose tissue–derived MSCs

We isolated MSCs from subcutaneous adipose tissue of male Sprague-Dawley rats on the basis of the adherent properties of these cells. We obtained $1.7 \times 10^5 \pm 0.2 \times 10^5$ cells from 1 g adipose tissue in a 12-h culture. By day 4 of culture of the minced adipose tissue, spindle-shaped adherent cells were apparent and formed symmetric colonies. After approximately three to four passages, most adherent cells expressed CD29 and CD90 (**Supplementary Fig. 1** online). In contrast, the majority of adherent cells were negative for CD34 and CD45. They were also negative for CD31, a marker for vascular endothelial cells, and negative for α smooth muscle actin (αSMA), a marker for smooth muscle cells. A small fraction of adherent cells expressed CD71, CD106 and CD117. These results were similar to those from bone marrow–derived MSCs[15,22,25] (**Supplementary Fig. 1** online). Using previously described methods[16,22,26], we confirmed that these adipose-derived adherent cells, like bone marrow–derived MSCs, were multipotent, as judged by their ability to differentiate into adipocytes, osteoblasts and vascular endothelial cells. Thus, we

[1]Department of Regenerative Medicine and Tissue Engineering, National Cardiovascular Center Research Institute and [2]Department of Pathology, National Cardiovascular Center, 5-7-1 Fujishirodai, Suita, Osaka, 565-8565, Japan. [3]Department of Cardiovascular Surgery, Okayama University Graduate School of Medicine, Dentistry and Pharmaceutical Sciences, 2-5-1 Shikata-cho, Okayama, 700-8555, Japan. [4]Department of Physiology, School of Medicine, Tokai University, Bohseidai, Isehara, Kanagawa, 259-1193, Japan. [5]Institute of Advanced Biomedical Engineering and Science, Tokyo Woman's Medical University, 8-1 Kawada-cho, Shinjuku-ku, Tokyo, 162-8666, Japan. [6]Department of Biochemistry, National Cardiovascular Center Research Institute and [7]Department of Cardiovascular Surgery, National Cardiovascular Center and [8]Department of Cardiac Physiology, National Cardiovascular Center Research Institute, 5-7-1 Fujishirodai, Suita, Osaka, 565-8565, Japan. [9]These authors contributed equally to this work. Correspondence should be addressed to N.N. (nnagaya@ri.ncvc.go.jp) or H.M. (hidemori@ri.ncvc.go.jp).

Received 9 August 2005; accepted 3 March 2006; published online 2 April 2006; doi:10.1038/nm1391

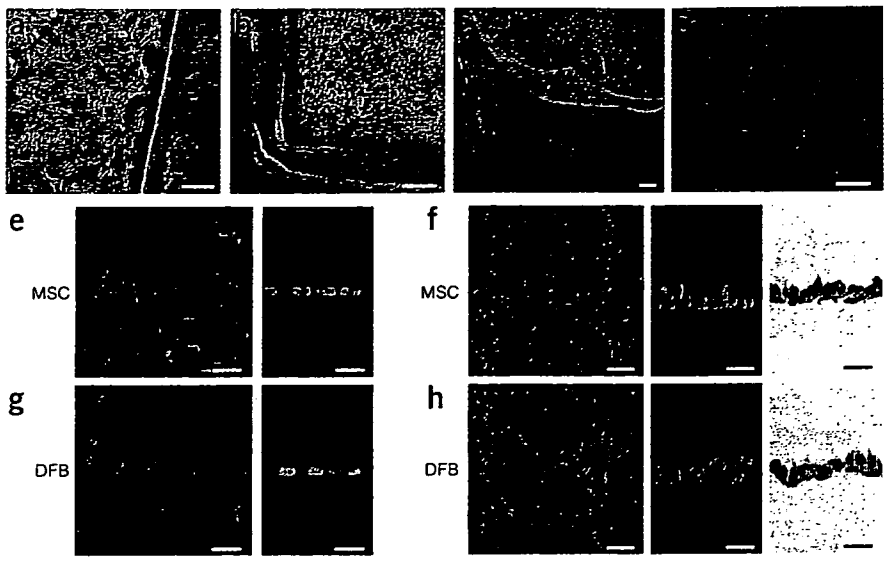

Figure 1 Preparation of monolayered MSCs. (a) MSCs 2 d after seeding on a temperature-responsive dish. (b) Cultured MSCs expanded to confluence within the square area of the dish by day 3. (c) The monolayered MSCs detached easily from the culture dish at 20 °C. (d) The completely detached monolayered MSCs were identified as a 12 × 12 mm square sheet. (e–h) Cross-sectional analysis of GFP-expressing monolayered MSCs and DFBs before detachment (e and g, confocal images) and after detachment (f and h, left and center, confocal images; right, Masson trichrome). The thickness of both monolayers was 3.5-fold greater than the thickness before detachment, and constituent cells were compacted. Scale bars in a–c, 100 μm; in d, 5 mm; in e–h, 20 μm.

confirmed that the majority of adherent cells isolated from adipose tissue were MSCs.

Preparation and transplantation of monolayered MSCs

We cultured adipose tissue–derived MSCs (5×10^5 cells) on temperature-responsive dishes for 3 d until confluent. MSCs were attached on the poly-*N*-isopropylacrylamide (PIPAAm)-grafted area (24 × 24 mm; **Fig. 1a,b**). As the culture temperature was decreased from 37 °C to 20 °C, MSCs detached spontaneously and floated up into the culture medium as a monolayer of MSCs within 40 min (**Fig. 1c,d**). As a control, we prepared dermal fibroblasts (DFBs) by the skin explant technique[27]. DFBs (8×10^5 cells) were cultured on the temperature-responsive dishes, and monolayered DFBs were fabricated as described above. The final cell counts for monolayered MSCs and DFBs before transplantation were $9.4 \pm 0.6 \times 10^5$ and $8.6 \pm 0.6 \times 10^5$ cells, respectively ($n = 6$ each). To identify the thickness of monolayered MSCs, we used green fluorescent protein (GFP)-expressing cell grafts derived from the GFP-transgenic Sprague-Dawley rats. Immediately after detachment, cells became compacted, possibly owing to cytoskeletal tensile reorganization, and the thickness of monolayered MSCs and DFBs was approximately 3.5-fold greater than the thickness before detachment (MSCs, 6.2 ± 0.3 to 21.5 ± 0.8 μm; DFBs, 6.5 ± 0.4 to 22.4 ± 1.1 μm; **Fig. 1e–h**). MSCs on the temperature-responsive dishes were positive for vimentin and slightly positive for collagen type 1, whereas DFBs were positive for both markers (**Fig. 2a**). We transferred detached monolayered MSCs above the myocardial scar (**Fig. 2b**) and then attached them to the surface of the anterior scar (**Fig. 2c**).

Secretion of angiogenic factors from monolayered MSCs

We measured secretion of angiogenic factors from MSCs 24 h after monolayers had formed, equivalent to day 4 after initial cell seeding. The monolayered MSCs secreted significantly larger amounts of angiogenic and antiapoptotic factors such as vascular endothelial growth factor (VEGF) and hepatocyte growth factor (HGF) than did the monolayered DFBs ($P < 0.01$; **Fig. 2d**). The control medium supplemented with 10% fetal calf serum contained less than 5 pg/ml of VEGF or HGF. These results suggest that the paracrine effects of monolayered MSCs on host myocardium are greater than those of monolayered DFBs.

Engraftment and growth of monolayered MSCs

To identify the transplanted cells in myocardial sections, we used GFP-expressing cell grafts derived from the GFP-transgenic Sprague-Dawley rats. We grafted monolayered MSCs or DFBs onto the scar area of the anterior wall (**Fig. 3**). Fluorescence microscopy showed that GFP-expressing monolayered MSCs gradually grew *in situ* and developed into a thick stratum, up to ~600 μm thick over the native tissue at 4 weeks (**Fig. 3a–f**). The engrafted MSC tissue tapered off toward the healthy myocardium (**Fig. 3d,e**), although most of the monolayered MSCs were attached only to the scar area in the anterior wall because of the large infarct. We rarely detected TUNEL-positive MSCs in the sheet (< 1%) 48 h after transplantation (**Fig. 3g**), implying that cell viability in the sheet was maintained. In contrast, we frequently detected TUNEL-positive cells (15% ± 2%) in the DFB sheet, which was observed as a thin layer above the scar. Subsequently, the DFB sheet was undetectable 1 week later. Masson trichrome staining showed increased thickness of the anterior wall and attenuation of left ventricle enlargement after transplantation of monolayered MSCs (**Fig. 3h**), although the infarct size did not differ significantly among the untreated, DFB and MSC groups (**Supplementary Table 1** online).

Reconstruction of cardiac mass

After growth *in situ*, GFP-expressing MSC tissue contained a number of mature vascular structures that had positive staining for von Willebrand factor (vWF) and αSMA (**Fig. 4a,b**). A small fraction of the MSC tissue had positive staining for cardiac troponin T and desmin (**Fig. 4c,d**). On the other hand, a large proportion of the MSC tissue was positive for vimentin, a marker for mesenchymal lineage cells (**Fig. 4e**). The percentages of graft-derived cells that expressed endothelial (vWF), smooth muscle (αSMA), cardiac (troponin T) and mesenchymal (vimentin) markers were 12.2% ± 0.6%, 5.0% ± 0.3%, 5.3% ± 0.3% and 57.8% ± 2.2%, respectively. Notably, based on expression of these markers, two-thirds of vascular endothelial cells, four-fifths of smooth muscle cells and one-twentieth of cardiomyocytes within the MSC tissue were GFP^- and hence were derived from the host. The MSC tissue stained modestly for collagen type 1 (**Fig. 4f**). Picrosirius red staining showed that collagen deposition was found mainly in the extracellular matrix and the epicardial margin of the MSC tissue (**Fig. 4g**). Excluding staining in blood vessels, the MSC tissue was also negative for αSMA, a marker for myofibroblasts (**Fig. 4b**). This phenotype was consistent with properties of MSCs

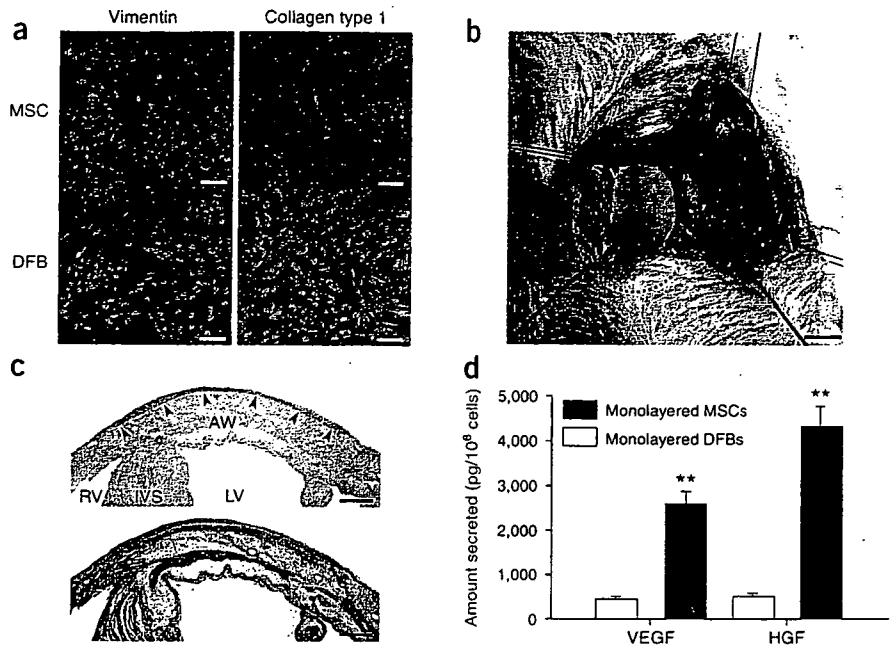

Figure 2 Characteristics of monolayered MSCs. (a) Properties of constituent cells in the monolayered grafts. Compared with DFBs (green), MSCs (green) are positive for vimentin (red) and slightly positive for collagen type 1 (red). (b) Monolayered MSCs (in the dotted circle) transferred to the infarcted heart. (c) Extent of monolayered MSCs 48 h after transplantation (arrows). AW, anterior wall; LV, left ventricle; RV right ventricle; IVS, interventricular septum. (d) Comparison of secretion of growth factors between monolayered MSCs and DFBs. $^{**}P < 0.01$ versus DFBs. Scale bar in a, 20 μm; in b, 5 mm; in c, 100 μm.

before transplantation (**Fig. 2a** and **Supplementary Fig. 1** online), suggesting that the MSC tissue includes a number of undifferentiated MSCs. Taken together, the grown MSC tissue was composed of newly formed blood vessels, undifferentiated MSCs and few cardiomyocytes.

Fluorescence *in situ* hybridization analysis

We performed fluorescence *in situ* hybridization (FISH) to detect X and Y chromosomes after sex-mismatched transplantation of monolayered MSCs. We transplanted GFP-expressing monolayered MSCs derived from male rats to female Sprague-Dawley rats that had suffered an infarct. Four weeks later, newly formed cardiomyocytes that were positive for GFP had only one set of X and Y chromosomes, whereas we detected two X chromosomes exclusively in GFP^- host-derived cells (**Fig. 4h**). We counted the X and Y chromosomes in male and female control rats and in the MSC sheet–transplanted rats (**Supplementary Table 2** online), and we did not detect extra copies of the X or Y chromosome in graft-derived GFP^+ cardiomyocytes. When we compared the frequencies of the occurrence of zero, one, two and more than two X chromosomes in the GFP^+ cardiomyocytes with the frequencies in male control cardiomyocytes, the GFP^+ cardiomyocytes did not show an increased proportion of X chromosomes ($0.25 > P > 0.10$, χ^2 test).

Effects of monolayered MSCs on cardiac function

Heart failure developed 8 weeks after coronary ligation, as indicated by an increase in left ventricle end-diastolic pressure (LVEDP) and attenuation of maximum and minimum rate of change in left ventricular pressure (dP/dt). Autologous transplantation of monolayered MSCs, however, resulted in decreased LVEDP (**Fig. 5a**). Left ventricle maximum and minimum dP/dt were significantly improved in the MSC group (**Fig. 5b,c**). We did not observe these hemodynamic improvements in the DFB group. The MSC group also had significantly lower right ventricular weight and lung weight than the DFB and untreated groups 4 weeks after transplantation (**Supplementary Table 1** online). These results suggest that transplantation of monolayered MSCs has beneficial hemodynamic effects in rats with chronic heart failure.

Echocardiographic analysis showed that transplantation of monolayered MSCs significantly increased diastolic thickness of the infarcted anterior wall (**Fig. 5d**). Left ventricle end-diastolic dimension at 8 weeks was significantly smaller in the MSC group than in the DFB and untreated groups (**Fig. 5e**). Transplantation of the monolayered MSCs significantly increased left ventricle fractional shortening (**Fig. 5f**). Left ventricle wall stress in diastole was markedly lower in the MSC group than in the DFB and untreated groups (**Supplementary Table 3** online). Plasma atrial natriuretic peptide (ANP) in the DFB and untreated groups was markedly elevated 8 weeks after myocardial infarction (**Fig. 5g**). Transplantation of the monolayered MSCs inhibited the increase in plasma ANP.

Survival analysis

The Kaplan-Meier survival curve showed that 4-week survival after coronary ligation did not differ significantly between the untreated and MSC groups before transplantation (**Fig. 5h**). Notably, however, no rats died after transplantation of monolayered MSCs. Therefore, the survival rate after transplantation was markedly higher in the MSC group than in the untreated group (4-week survival after transplantation was 100% for the MSC group versus 71% for the untreated group, log-rank test, $P < 0.05$).

DISCUSSION

There are several advantages to monolayered MSC transplantation. First, the self-propagating property of MSCs *in situ* leads to the formation of a thick stratum on the surface of the scarred myocardium. Second, the multipotency of MSCs and their ability to supply angiogenic cytokines allows neovascularization in the MSC tissue. Third, the reconstruction of thick myocardial tissue reduces left ventricle wall stress and results in improvement of cardiac function after myocardial infarction. Finally, a substantial part of the transplanted tissue is composed of undifferentiated MSCs, and it is tempting to speculate that such cells may act against future progressive left ventricle remodeling.

Cellular cardiomyoplasty using needle injections is emerging as a treatment option for individuals with chronic heart failure, but it may be limited by failure to regenerate cardiac mass. The cell sheet allows for cell-to-cell connections owing to the lack a need for enzymatic digestion[6–10]. Thus, the cell sheet has attracted considerable interest as a tool for tissue engineering[28]. Here, we used adipose tissue–derived MSCs as a cellular source for the cell sheet, which resulted in successful autologous transplantation in heterogenic rats without immunological

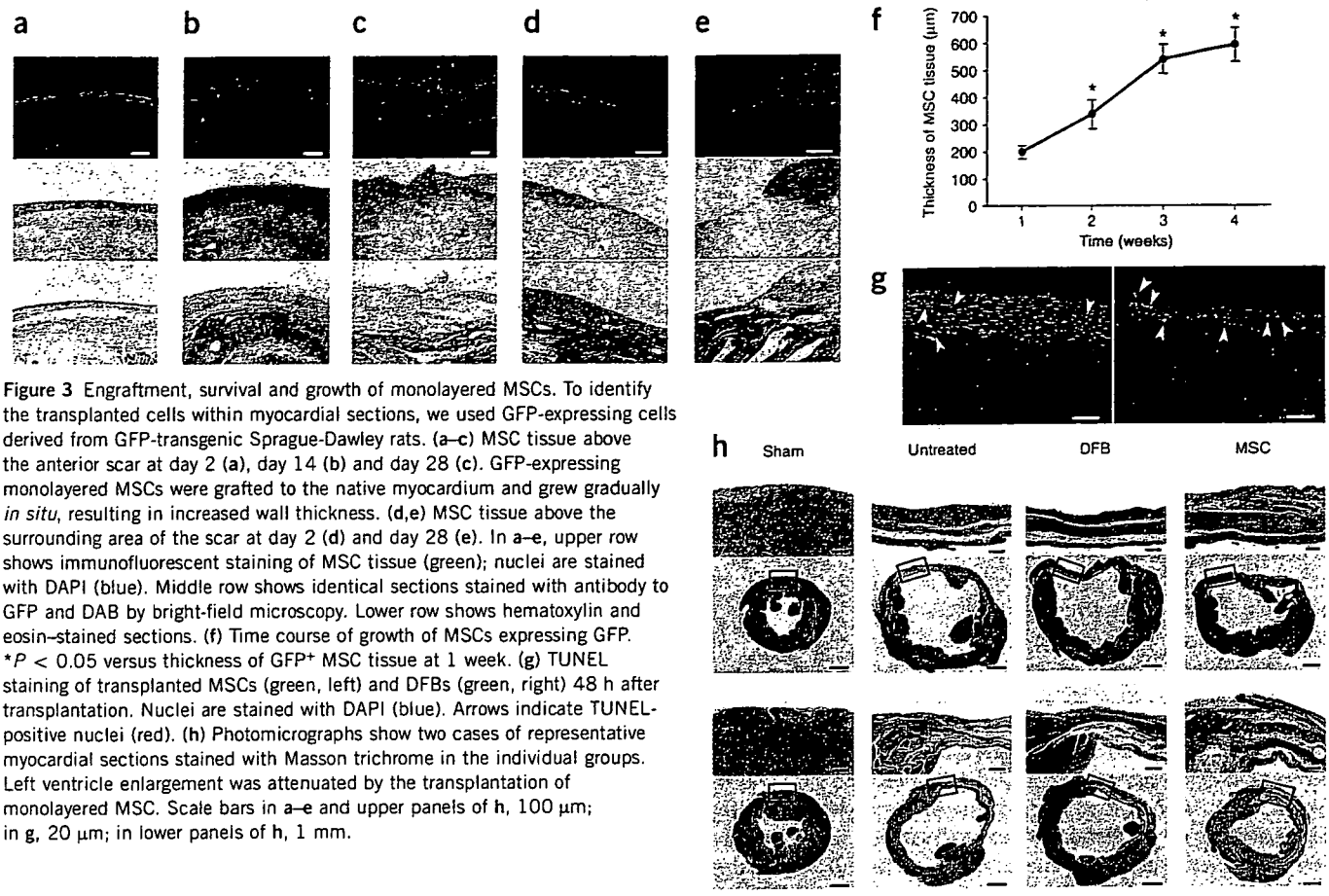

Figure 3 Engraftment, survival and growth of monolayered MSCs. To identify the transplanted cells within myocardial sections, we used GFP-expressing cells derived from GFP-transgenic Sprague-Dawley rats. (a–c) MSC tissue above the anterior scar at day 2 (a), day 14 (b) and day 28 (c). GFP-expressing monolayered MSCs were grafted to the native myocardium and grew gradually *in situ*, resulting in increased wall thickness. (d,e) MSC tissue above the surrounding area of the scar at day 2 (d) and day 28 (e). In a–e, upper row shows immunofluorescent staining of MSC tissue (green); nuclei are stained with DAPI (blue). Middle row shows identical sections stained with antibody to GFP and DAB by bright-field microscopy. Lower row shows hematoxylin and eosin–stained sections. (f) Time course of growth of MSCs expressing GFP. $^*P < 0.05$ versus thickness of GFP$^+$ MSC tissue at 1 week. (g) TUNEL staining of transplanted MSCs (green, left) and DFBs (green, right) 48 h after transplantation. Nuclei are stained with DAPI (blue). Arrows indicate TUNEL-positive nuclei (red). (h) Photomicrographs show two cases of representative myocardial sections stained with Masson trichrome in the individual groups. Left ventricle enlargement was attenuated by the transplantation of monolayered MSC. Scale bars in a–e and upper panels of h, 100 μm; in g, 20 μm; in lower panels of h, 1 mm.

rejection. Using flow cytometry, we did not find any substantial differences between adipose tissue–derived MSCs and bone marrow–derived MSCs, consistent with results from previous studies[22,25]. Adipose-derived MSCs readily attached to and propagated on the temperature-responsive dish. Abdominal subcutaneous adipose tissue is clinically redundant and easily accessible by rapid and minimally invasive surgery such as liposuction. Thus, adipose tissue may serve as a source of stem cells for therapeutic cell sheets.

Here, monolayered MSCs could readily be transferred and grafted to the scarred myocardium without additives or suturing. This may be attributable to cell-to-cell connections as well as extracellular matrix deposits on the basal surface of the monolayered MSCs. Regeneration of myocardial mass is thought to require multilayered constructs of the cell sheet. Unfortunately, however, the lack of a vascular network has limited the formation of a thick construct[10,29]. The transplanted monolayered MSCs thickened gradually, developing into a stratum of up to 600 μm in thickness over the native tissue 4 weeks after transplantation, suggesting that monolayered MSCs have an ability to grow *in situ*. As a result, the transplanted MSC tissue reversed wall thinning of the infarcted myocardium. On the other hand, the fibroblast sheet did not grow *in situ*. It should be noted that the MSC tissue included a large number of newly formed blood vessels. These vessels were composed of graft-derived cells, host-derived cells or both. The MSC sheet secreted a large amount of angiogenic and antiapoptotic cytokines, including VEGF and HGF, as compared with the fibroblast sheet. These results suggest that MSCs induce neovascularization within the sheet not only through their ability to differentiate into vascular cells but also through growth factor–mediated paracrine regulation. Thus, we believe that the angiogenic action of MSCs is important for reconstruction of cardiac mass by the MSC tissue.

Four weeks after transplantation, a small fraction of the engrafted MSCs were positive for cardiac proteins such as cardiac troponin T and desmin, suggesting the presence of cardiomyocytes within the MSC tissue. FISH analysis suggested that the most cardiomyocytes within the MSC tissue were not derived from cell fusion, but we are unable to exclude the possibility that some were. Further studies are necessary to investigate the mechanisms by which MSCs within the MSC tissue regenerate cardiomyocytes. The majority of the MSC tissue was positive for vimentin, a marker for undifferentiated MSCs and fibroblasts. In addition, the majority of MSCs within the graft were negative for collagen type 1 and αSMA, a marker for myofibroblasts. These results suggest that the grown-up MSC tissue is composed of newly formed blood vessels, undifferentiated MSCs and few cardiomyocytes.

We have also shown that transplantation of the monolayered MSCs significantly increased left ventricle maximum dP/dt, decreased LVEDP and inhibited the development of left ventricle enlargement in rats with chronic heart failure secondary to myocardial infarction. These results suggest that transplantation of monolayered MSCs improves cardiac function. But the presence of cardiomyocytes within the MSC tissue seemed to be rare. Thus, this improvement may be explained mainly by growth factor–mediated paracrine effects of the MSC sheet and a decrease in left ventricle wall stress resulting from the thick MSC tissue. Furthermore, no rats treated with the monolayered MSCs died during the study period, although untreated rats died frequently. These results indicate that fatal arrythmogenic problems were not caused by integration of the MSC tissue.

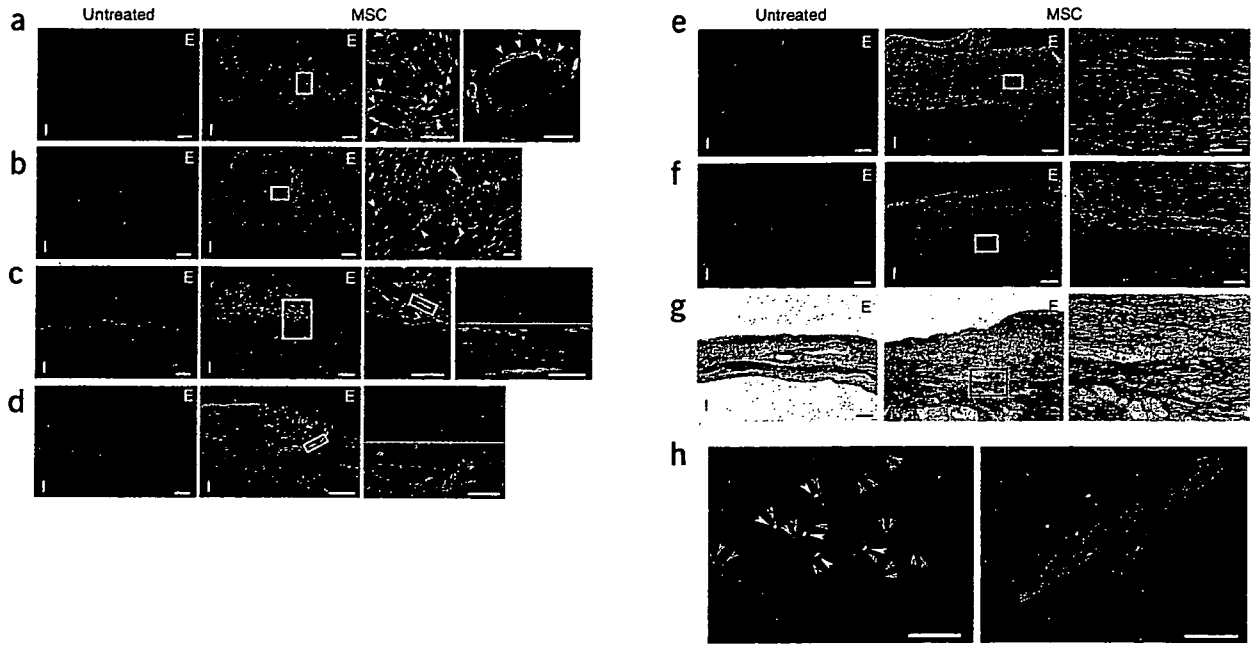

Figure 4 Differentiation of MSCs within the MSC tissue after growth *in situ*. (**a**,**b**) GFP-expressing MSCs (green) were identified as a thick stratum at the epicardial side of the myocardium. The MSC tissue contained a number of vascular structures positive for vWF (red, **a**) and αSMA (red, **b**). MSCs that did not participate in blood vessel formation were only rarely positive for αSMA, a marker for myofibroblasts. Arrows indicate transplanted MSCs positive for vWF or αSMA. (**c**,**d**) Some MSCs within the MSC tissue were positive for cardiac markers cardiac troponin T (red, **c**) and desmin (red, **d**). (**e**) Most of the MSC tissue was positive for vimentin (red). (**f**) The MSC tissue modestly stained for collagen type 1 (red). (**g**) Collagen deposition was also detected by picrosirius red staining. (**h**) FISH analysis. Newly formed cardiomyocytes (desmin, red) that were positive for GFP (green) had only one set of X (purple) and Y chromosomes (white), whereas two X chromosomes were detected exclusively in GFP^- host-derived cells. Nuclei are stained with DAPI (blue, **a**–**f** and **h**). Scale bars in left three panels of **a** and **c** and in two left panels of **b** and **d**–**g**, 100 μm; in **h** and far right panels of **a**–**g**, 20 μm. E, epicardial side; I, intimal side.

In summary, adipose tissue–derived monolayered MSCs can be readily engrafted to the scarred myocardium, grow gradually *in situ* and become a thick stratum that includes newly formed vessels, cardiomyocytes and undifferentiated MSCs. The engrafted MSCs reversed wall thinning in the scar area and improved cardiac function and survival in rats with myocardial infarction. Thus, transplantation of monolayered MSCs may be a new therapeutic strategy for cardiac tissue regeneration.

METHODS

Model of heart failure. All protocols were performed in accordance with the guidelines of the Animal Care Ethics Committee of the Japanese National Cardiovascular Center Research Institute. We used male Sprague-Dawley rats (Japan SLC) weighing 187–215 g. A myocardial infarction model was produced by ligation of the left coronary artery, as described previously[30]. Briefly, we anesthetized rats with sodium pentobarbital (30 mg/kg) and ventilated them with a volume-regulated respirator. We exposed hearts by left thoracotomy, and ligated the left coronary artery 2–3 mm from its origin between the pulmonary artery conus and the left atrium with a 6-0 Prolene suture. The sham group underwent thoracotomy and cardiac exposure without coronary ligation. The surviving rats were maintained on standard rat chow.

Study protocol. We randomly placed rats into four groups: rats with chronic heart failure that underwent transplantation of monolayered MSCs (MSC group; $n = 12$), rats with chronic heart failure given monolayered DFBs (DFB group; $n = 12$), rats with chronic heart failure without transplantation (untreated group; $n = 12$) and sham-operated rats without transplantation (sham group; $n = 10$). Four weeks after coronary ligation, the MSC and DFB groups underwent autologous transplantation of each monolayered cell graft onto the anterior wall, including the scar area (**Supplementary Methods** online). The other two groups underwent the same operative procedures without transplantation. We performed hemodynamic studies, echocardiography and histological assessments 4 and 8 weeks after coronary ligation (**Supplementary Methods**). Upon killing at 8 weeks after coronary ligation, only those rats with infarct size > 25% of the left ventricle area were included in this study. Therefore, the variation in infarct size between the experimental rats was relatively low (28–41%, average 33.9% ± 1.9%).

Isolation and culture of MSCs from adipose tissue. Immediately after coronary ligation, we acquired subcutaneous adipose tissue (1.1 ± 0.1 g) from the right inguinal region of each rat. We minced adipose tissue with scissors and digested it with 10 ml of type 1 collagenase solution (0.1 mg/ml, Worthington Biochemical) for 1 h in a 37 °C water bath shaker. After filtration with mesh filter (Costar 3480, Corning) and centrifugation at 780*g* for 8 min, we suspended isolated cells in α-MEM supplemented with 10% FCS and antibiotics, plated them onto a 100-mm dish and incubated them at 37 °C with 5% CO_2. A small number of spindle-shaped cells were apparent in visible symmetric colonies by days 5–7.

Preparation of temperature-responsive dishes. Specific procedures for preparation of square-designed PIPAAm-grafted dishes have been previously described[9]. Briefly, we spread IPAAm monomer (Kohjin) in 2-propanol solution onto 60-mm polystyrene culture dishes (Corning). We then subjected the dishes to irradiation (0.25-MGy electron beam dose) using an Area Beam Electron Processing system (Nisshin High-Voltage) to immobilize IPAAm on the dish surface; we then rinsed dishes with cold distilled water and dried them in nitrogen gas. In the second step, we masked the PIPAAm-grafted surface with a square glass coverslip (24 × 24 mm, Matsunami Glass). We spread acrylamide (AAm) monomer solution in 2-propanol onto the masked dish surface. We then irradiated the dish surface with an electron beam and washed it. As a result, the central square area of each dish was PIPAAm grafted (temperature responsive), and the surrounding border was poly-AAm grafted (non–cell adhesive). This PIPAAm-grafted surface is hydrophobic under culture